

HYPOBATT

Hyper powered vessel battery charging system

Document type **Deliverable**

Document number **D2.1**

Primary Author(s) Paulo Cardoso | BRING

Document Version | Status 2.0 | Final

Distribution level PUB - PUBLIC

Project Acronym **HYPOBATT**

Project Title **Hyper Powered vessels battery charging system**

Project website WWW.HYPOBATT.COM

Project Coordinator Endika Bilbao | IKE | ebilbao@ikerlan.es

Grant agreement number 101056853

Date of deliverable: [29.03.2023]

Date of submission: [31.03.2023]



©HYPOBATT has received funding from the European Horizon Europe Framework Programme (HORIZON) under grant agreement No. 101056853. This reflects only the author's views. The Agency is not liable for any use that may be made of the information contained therein

Copyright © all rights reserved. This document or any part thereof may not be made public or disclosed, copied or otherwise reproduced or used in any form or by any means, without prior permission in writing from the HYPOBATT Consortium. Neither the HYPOBATT Consortium nor any of its members, their officers, employees, or agents shall be liable or responsible in negligence or otherwise for any loss, damage or expense whatever sustained by any person as a result of the use, in any manner or form, of any knowledge, information or data contained in this document, or due to any inaccuracy, omission or error therein contained.

CONTRIBUTOR AND FORMAL REVIEWERS

	Name Organisation	Date
Document Manager	Paulo Cardoso (BRING)	16/03/2022
Contributor 1	Mohsen Akbarzadeh (FM)	07/03/2023
Contributor 2	Remi De Coster (FM)	08/03/2023
Contributor 3	Jeroen Zwysen (FM)	09/03/2023
Contributor 4	Thai Phuong Do (CEA)	27/02/2023
Contributor 5	Gondat Manex (IKE)	03/03/2023
Contributor 6	Bilbao Endika (IKE)	17/02/2023
Contributor 7	Elezgarai Gorka (IKE)	17/02/2023
Contributor 8	Claudio Langella (RINA)	16/02/2023
Reviewer 1	Bilbao Endika (IKE)	21/03/2023
Reviewer 2	George Kostalas (RHOE)	23/03/2023
Reviewer 3	Peter Grippi (STT)	29/03/2023
Reviewer 4	Maraike Pommer (Frisia)	29/03/2023

DOCUMENT HISTORY

Document Version	Date	Author Organization	Description
0.1	2022-10-03	Paulo Cardoso (BRING)	Initial version
1.0	2023-03-16	Paulo Cardoso (BRING)	First internal released version
1.1	2023-03-23	Paulo Cardoso (BRING)	Internal Reviewed version
1.2	2023-03-29	Paulo Cardoso (BRING)	External Reviewed version
1.5	2023-03-29	Paulo Cardoso (BRING)	Edited final version
2.0	2023-03-29	Paulo Cardoso (BRING)	Final version – Submitted to EC


Approval Status			
	Organisation Name	Checked By	Approved
WP Leader Approval	RHOE	Georgios Kostalas	Date: 30.03.2023 Signature: 

Table of contents

Table of contents	3
1. EXECUTIVE SUMMARY	8
2. OBJECTIVES	9
3. INTRODUCTION	10
4. DESCRIPTION OF WORK	12
4.1 Battery System Models	12
4.1.1 Electro-Thermal model	12
4.1.2 Battery model inputs and outputs	14
4.1.3 Aging model	15
4.1.4 Safety considerations	18
4.1.5 Connection setup to the charger	19
4.2 Vessel MW Charger Models – Transformer	19
4.2.1 Transformer electrical model	20
4.2.2 Thermal model	21
4.2.3 Implementation and safety considerations	24
4.3 Vessel MW Charger Models - Converter	25
4.3.1 Major components data for initial modelling	25
4.3.2 Charger inputs and outputs	29
4.3.3 Safety considerations	29
5. Vessel MW Charger Models – Scalability & Optimization	30
5.1.1 Scalability towards multiple transformers & converters	30
5.1.2 Optimization speed towards large scale simulation	30
5.2 Grid Model	33
5.2.1 Architecture and evolution	34
5.2.2 Component models	35
6. Digital twin and Use cases example	41
7. CONCLUSIONS	43
8. References	45

LIST OF ABBREVIATIONS, ACRONYMS AND DEFINITIONS

Abbreviation	Word
BMS	Battery Management System
CC	Constant Current
CV	Constant Voltage
DoD	Depth of discharge
DT	Digital Twin
ECM	Equivalent Circuit Model
EMS	Energy Management System
EV	Electric Vehicle
FRT	Fault Ride Through
HPPC	Hybrid Pulse Power Characterization
IoT	Internet of Things
OCV	Open Circuit Voltage
PV	Photovoltaic
SOC	State-of-Charge

LIST OF TABLES

Table 1 Electrical parameters needed for the model.....	13
Table 2 Thermal parameters needed for the model.....	14
Table 3 Transformer parameters needed from the manufacturer for the electrical model.....	21
Table 4 Nusselt number analytical equations.....	23
Table 5 Speed optimization towards large scale simulation.....	30
Table 6 Simulation times with described speed optimizations.....	32
Table 7 Simulation times when optimizing the electrical/magnetic transformer model.....	33
Table 8 PV parameters.....	37
Table 9 Grid parameters.....	40
Table 10 Battery parameters used in the use cases.....	41

LIST OF EQUATIONS

Equation 1 Heat generation equation.....	13
Equation 2 General form of a cycle life equation.....	15
Equation 3 Parameterized cycle life equation of a battery.....	15
Equation 4 Impact of DoD on nCL.....	16
Equation 5 Temperature stress factor.....	17
Equation 6 SOC stress factor.....	17
Equation 7 C-rate stress factor.....	18
Equation 8 Conduction resistance.....	22
Equation 9 Convection resistance.....	22
Equation 10 Heat transfer coefficient equation.....	23
Equation 11 Grashof number equation.....	23
Equation 12 Prandtl number equation.....	23
Equation 13 Radiation resistance equation.....	24

LIST OF FIGURES

Figure 1 Overall architecture of the Digital Twin.....	10
Figure 2 Simulink battery model.....	12
Figure 3 Rint model schematic. Adapted from [23].....	13
Figure 4 Thermal Model equivalent circuit used. Adapted from [24].....	14
Figure 5 Battery model inputs and outputs.....	15
Figure 6 FEC versus DOD for NMC chemistry [6].....	16
Figure 7 Aging stress factor related to DoD.....	16
Figure 8 Aging stress factor related to temperature [7].....	17
Figure 9 Aging stress factor related to SOC _{avg}	17
Figure 10 Aging stress factor related to C-rate.....	18
Figure 11 Single phased three windings transformer electrical model.....	20
Figure 12 General view of the converter model.....	25
Figure 13 Corner-ground mid-point two parallel connected AC/DC rectifiers.....	26
Figure 14 Thermal model: (a) Cauer model [14], (b) converter model's equivalent thermal circuit.....	27
Figure 15 Battery voltage and current waveforms during charging (unit test).....	27
Figure 16 Grid current waveforms at the beginning of the charging.....	28
Figure 17 Converter switches junction temperature.....	28
Figure 18 The generated different model levels; <Averaging window width>.....	28
Figure 19 Output voltage waveform example of a switched converter leg (left) and an average converter (right).....	29
Figure 20 Charger model inputs and outputs.....	29
Figure 21 Converter operation by ideal current sources.....	31
Figure 22 Battery voltage and current with the speed optimized model.....	32
Figure 23 Converter losses with the speed optimized model.....	33
Figure 24 Transformer losses with the speed optimized model.....	33
Figure 25 Electrical diagram in Norddeich port.....	35
Figure 26 Model of Norddeich port power grid with Simscape.....	35
Figure 27 Model of public grid connection.....	36
Figure 28 Model of the line.....	36
Figure 29 Example of FRT grid codes. Adapted from [17].....	38
Figure 30 Transformer model and parameters.....	39
Figure 31 Dynamic load model.....	39
Figure 32 Grid model inputs and outputs.....	40
Figure 33 Simulink model of the digital twin of the whole system.....	41
Figure 34 Voltage behaviour for the two use cases.....	42
Figure 35 SoC evolution for the two use cases.....	43
Figure 36 Charging current profile used in the two use cases.....	43

1. EXECUTIVE SUMMARY

In this report the developed Digital Twin (DT) of the parties that are acting on the physical world is presented. Three sub models were developed: one for the battery, other for the charger and one final for the grid. Some test runs were done with approximated parameters in the models of the real system and are presented in this deliverable using the case scenarios established in previous deliverables. With this first iteration the foundation is built, which will allow for further improvements on the following months, with the correct model parametrization and potential added features as it might be fit on the long run. This will be relevant to integrate in the cloud platform posteriorly at a later stage of the project.

Keywords: Digital Twin, Battery Modelling, Charger Modelling, Grid Modelling, IoT, cloud platform

2. OBJECTIVES

Main objective: To develop a DT composed of the three main active components of the future electrified Port system, Vessel twin, Charger twin and Grid twin. Overview of the parameter inputs that are needed for each model. Present a first iteration of the DT with all three components integrated and two (best and worst) case scenarios in terms of charging aiming to define a design process, which can be used to find the proper electric vessels and fast-charging infrastructure solutions for any given situation. Its sub-models will allow to identify the minimum and maximum boundaries of each component and subsystem in charger, vessel, and electric grid in ports. It can support the development of scalable sub-models that will be integrated and emerged together in the platform and will provide a performance validation through use case simulations with a generic charging profile. Not only to increase the performance efficiency but also optimize TCO of operational electrified vessels and potential ports and provide feasibility assessment towards widespread deployment of fast high power electrical charging.

This will be integrated online to a cloud solution to do online simulations, optimize the overall performance and daily operation plans of the system according to the defined requirements and provide flexibility to any specific EMS needed.

Additional objectives:

- Present a first iteration of the DT with all three components integrated.
- Overview of the parameter inputs that are needed for each model.
- Presentation of the two (best and worst) case scenarios in terms of charging requirements in terms of battery response to a charging event dependent on the current profile

3. INTRODUCTION

With the pursuit of the electrification of every transport sector, more and more emphasis are being placed on the biggest constrain of the process: the batteries. To provide functional, affordable, and competitive electric vehicles/vessels, batteries need to be safe, provide similar total power output per charging event to their fuel-based counterparts, allow for low charging times and have a long durability [1]. Given their non-linearity and complex behaviour, batteries present themselves as a difficult system to properly model and manage, making it hard to meet all the requirements [2]. More and more complete models have been developed to estimate battery parameters and states more accurately, but they are all limited by 1) amount of data they are receiving from the physical components and 2) lack of capability to process big amounts of data.

One of the ways of providing a solution to these two issues is through the use of a DT. Connecting both physical and virtual systems providing a big influx of data and parameters which will allow proper real time data monitoring of the batteries current and future response. The monitoring and management of the physical system is done in a cloud-based manner, with all information being fed into a cloud platform which will be responsible for its processing and to give an output to both physical and virtual components of the DT. This feedback will realize the expected optimizations and modifications [3]. The entire process will make use of the Internet of Things (IoT) concept to facilitate communication and transmission of data.

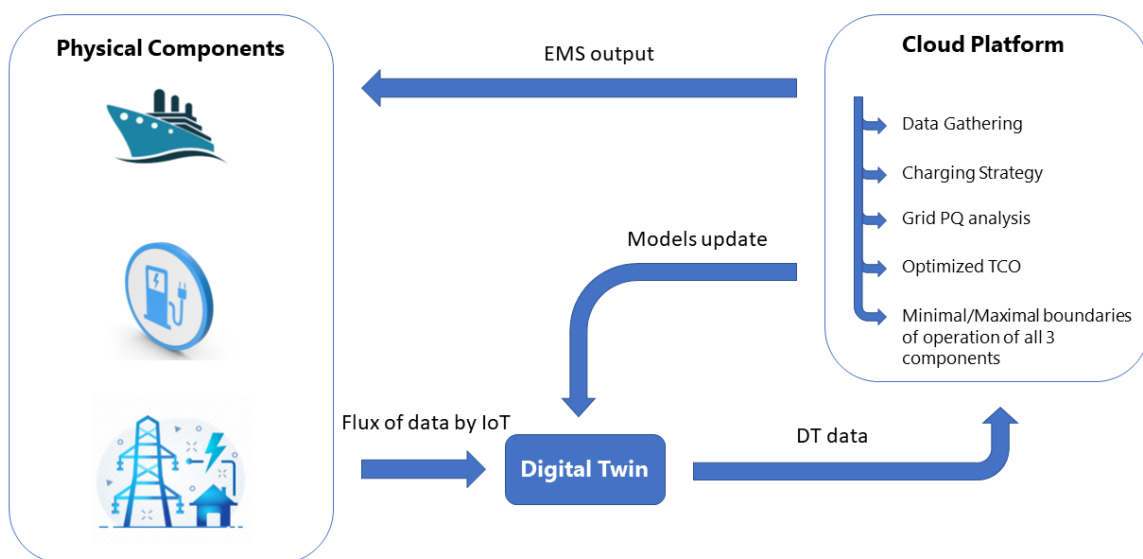


Figure 1 Overall architecture of the Digital Twin.

Directing into this project, the DT is composed of three components: battery, charger, and grid. Data from the ship's batteries, charger and grid are transmitted through the virtual twin, that

provides its own outputs combined with the ones received. Figure 1 gives an overview of the architecture of all interfaces.

With the DT, it will be possible to estimate with high precision the amount of power required from the grid, when this power needs to be deployed, how can this power be optimized energy and financially wise and with regards to the conservation of the battery's health. With an algorithm constantly learning through the inputs of the real system, more and better predictions will be done with time, leading to cost saving, battery preservation and port operation optimization.

4. DESCRIPTION OF WORK

4.1 Battery System Models

Battery modelling was done by a combination of two models: electrical and thermal model. These are interconnected and dependent on each other.

Because the vessel already has an incorporated battery management system (BMS) with a cell balancing algorithm, some simplifications were done:

- The entire battery system of the vessels was simplified to a single cell element.
- The thermal model was simplified to a 1D node array.

4.1.1 Electro-Thermal model

The electrical model is a table based equivalent circuit model (ECM). These models make use of electrical components to simulate dynamic characteristics of a battery under all operational scenarios. There is a multitude of ECM type models in the literature, arising from the simplest Rint model to the more complex multi-order models. Depending on the final objective of the model and the type of cell chemistry in study, different versions of ECMs can be deployed that better adapt to the electric response of the cell. For this application in specific the simpler Rint model was used as it provides the enough fidelity for its purpose and greatly reduces the computational burden of the DT. As mentioned in the previous section, the model was simplified to just one battery. This was achieved by adjusting the real capacity to a system that would demand the same power output from the charger. Its structure can be seen in Figure 2.

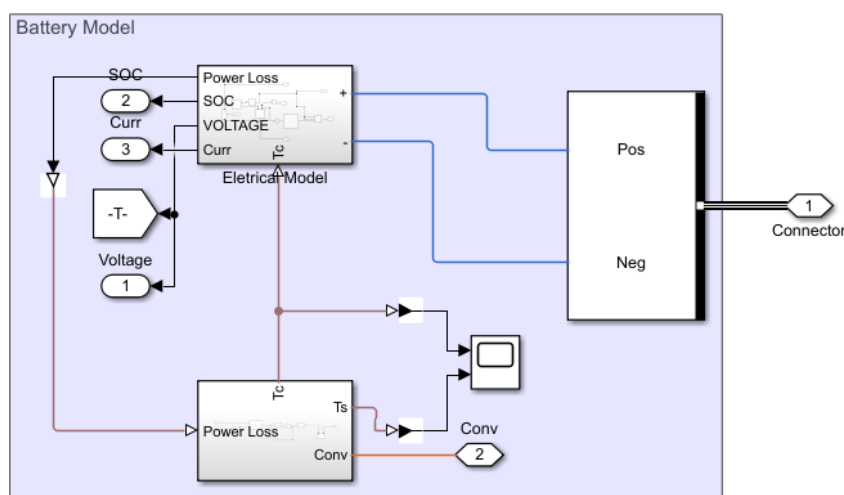


Figure 2 Simulink battery model.

To make the model as close to the real system as possible, experimental testing must be done to the batteries as a means to provide inputs to the model's parameters. The following data is needed.

Table 1 Electrical parameters needed for the model.

Electrical Battery Model Parameters
Open Circuit Voltage (OCV) as function of State-of-Charge (SOC) and temperature
Internal resistance as function of SOC and temperature
Battery system Capacity

This data can be provided either by the cells manufacturer or obtained by in-house characterization with OCV testing and Hybrid Pulse Power Characterization (HPPC) for the internal resistance. At the present moment approximate values obtained from literature with cells of the same chemistry and similar capacity are being used to assess the functionality of the DT, which will be compared with experimental data responses to a load profile to be presented.

The thermal model is a 1D nodal based model. An equivalence is made between the thermal properties and behaviour and an electrical circuit to simulate heat transfer phenomena.

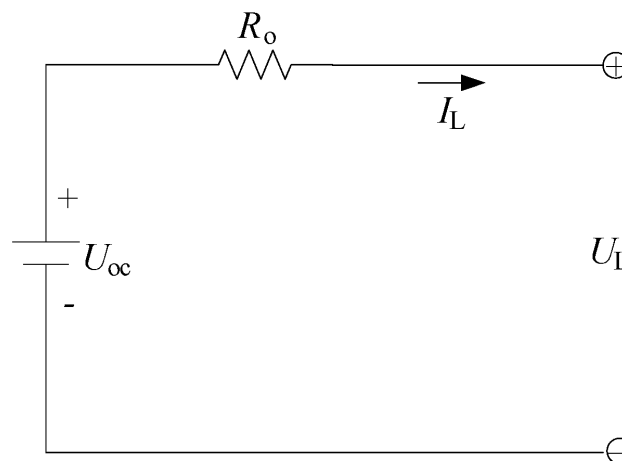


Figure 3 Rint model schematic. Adapted from [23].

Considering the simplification done in the electrical model, the same was done for the thermal, where one node represents the internal parameters of the entire battery system as means of them. A central node where the thermal mass is located is connected to a superficial node by means of a thermal resistance. A convective connection between the surface and the ambient is done as well. The power loss from the electrical model comes as an input for the heat generation of the central node. The usual equation for the heat generation inside a battery [4] is given by:

$$\dot{Q} = I \left(V - V_{oc} - T_{ref} \frac{dV_{oc}}{dT} \right)$$

Equation 1 Heat generation equation.

Where I represents the current through the cell, $V - V_{oc}$ is the heat generation from the Joule effect by means of the difference between the terminal voltage and the open circuit voltage, the second part, responsible for the reversible heat generation in the form of variation of entropy and T_{ref} is the reference temperature in which $\frac{dV_{oc}}{dT}$ was determined. In the model only the irreversible heat generation was considered given its major contribution in the heat generation component.

A temperature source of the ambient temperature is also established to constantly interact with the surface node. The ambient temperature will be directly dependent on the type of cooling system present in the vessel, and for that reason is disregarded in this first iteration. These connections are all done by thermal resistances which values can be determined analytically. Same can be said regarding the heat mass of the whole system. The structure can be seen in Figure 4. In order to properly determine the circuit parameters, the following data is necessary.

Table 2 Thermal parameters needed for the model.

Thermal Battery Model Parameters
Anisotropic thermal conductivity
Battery system dimensions
Heat transfer coefficient

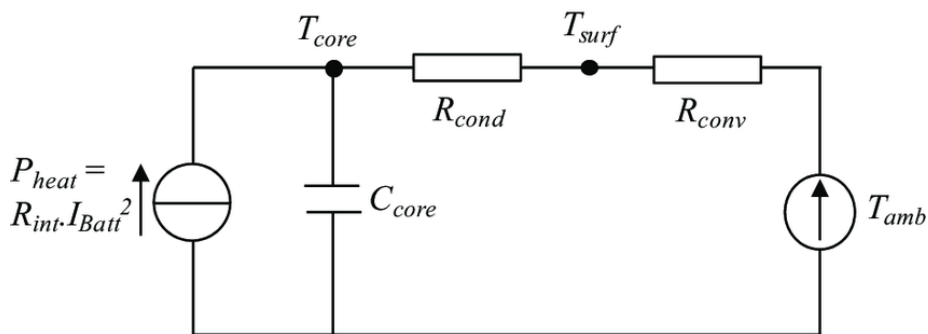


Figure 4 Thermal Model equivalent circuit used. Adapted from [24].

4.1.2 Battery model inputs and outputs

The battery model will make use of the SoC and temperature as initial inputs for a charging event. These setpoints will establish how much current needs to be provided in the first charging phase. After that, the battery model will be receiving the electrical current from the charger model. With these, the model is capable of fully simulate the vessel charging. Monitoring will be the main objective of the outputs, which depending on their value will allow to optimize not only the charging but also the DT itself to further enhance its capabilities.

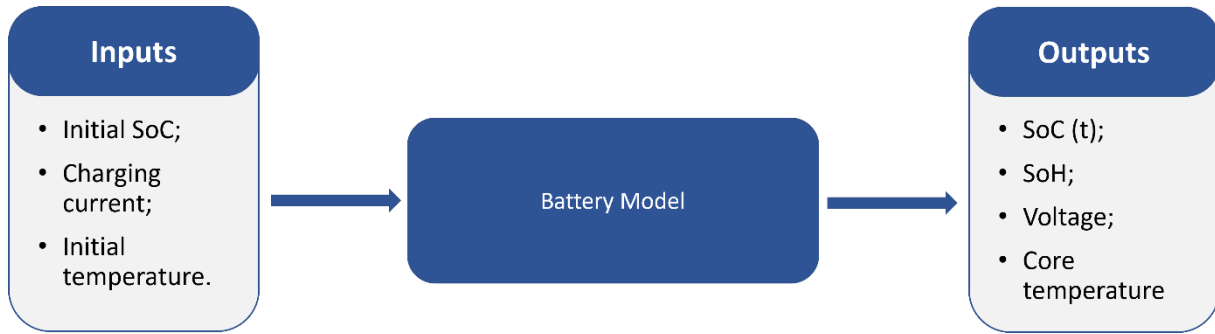


Figure 5 Battery model inputs and outputs.

4.1.3 Aging model

In this section, a generic e multi-factor cycle life prediction methodology for battery is presented. The developed aging model is a parameter driven aging model, which predicts the number of cycles that a battery can perform before reaching its end of life (losing 20% of its capacity) under a specific operational condition. Assuming a uniform cycle degradation of the battery along the lifetime, this model allows to obtain the percentage of the capacity fade of the battery for a certain number of cycles.

This model estimates the cycle life of the battery considering four aging factors related to cycle aging of the battery including:

- Depth of discharge (DoD)
- Average state of charge (SOC_{avg})
- Temperature (T)
- C-rate

The model estimates battery cycle life utilizing battery degradation stress factor models. In this model it is assumed that the impact of aging factors is independent of each other. Based on this independence assumption, the cycle life of the battery under a given cycling parameters, is written as follows [5].

$$\frac{CL(x_1, \dots, x_k)}{CL(x_{1,nom}, \dots, x_{k,nom})} = \frac{CL(x_1)}{CL(x_{1,nom})} \times \dots \times \frac{CL(x_k)}{CL(x_{k,nom})}$$

Equation 2 General form of a cycle life equation.

The index *nom* refers to nominal cycle life and cycling parameters, as found for example in a battery data sheet or gained from a cycling experiment for a single set of cycling parameters. Considering the aging factors of DoD, SOC_{avg} , T, and C-rate, the battery cycle life model is formulated as below:

$$CL(T, I_{dis}, I_{ch}, DOD, SOC_{ave}) = CL_{nom} \times nCL(T) \times nCL(I_{dis}) \times nCL(I_{ch}) \times nCL(DOD) \times nCL(SOC_{ave})$$

Equation 3 Parameterized cycle life equation of a battery.

where nCL is each associated normalised cycle life fraction.

Each stress factor mentioned in the previous section is determined based on the existing data in the literature. In this regard, the existing data on cycle aging of NMC cell type are collected from various sources.

4.1.3.1 Depth of Discharge (DoD)

The model of stress factor related to DoD is developed based on the experimental test results of Ecker et al. [6]. Figure 6 FEC versus DOD for NMC chemistry . shows the equivalent full cycles (FECs) versus DoD based on the experimental tests at different average state of charge values at 35°C.

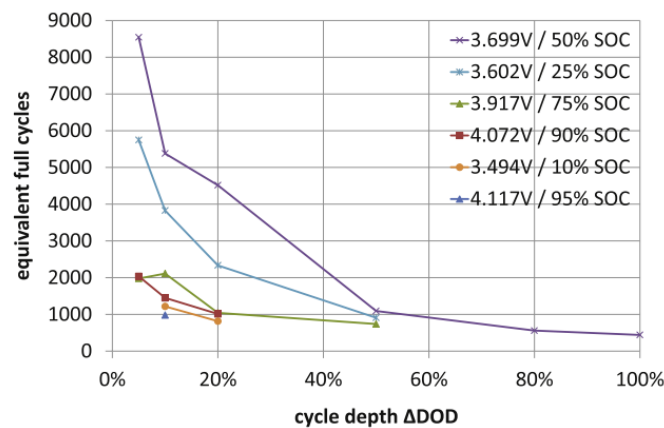


Figure 6 FEC versus DOD for NMC chemistry [6].

By fitting an exponential equation to the results for $SOC_{avg}=50\%$, the aging factor related to DoD is obtained (Figure 7).

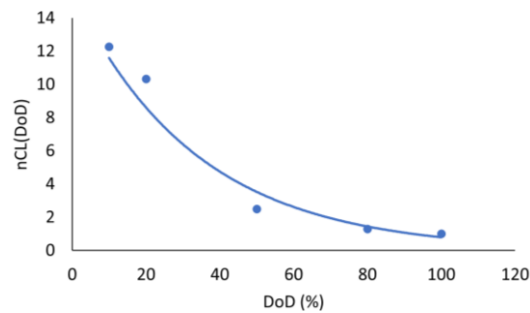


Figure 7 Aging stress factor related to DoD.

The fitted equation regarding the impact of DoD on nCL (DoD) is found as below:

$$nCL(DoD) = 15.601 \times e^{-0.03 \text{ DoD}}$$

Equation 4 Impact of DoD on nCL .

4.1.3.2 Temperature (T)

The impact of temperature on cycle life of NMC cell from various experimental works are collected in [7], as shown in Figure 8. As it is seen, the cycle life is maximum once the

temperature is between 20 – 25 °C. The temperature out of this scope leads to the reduction of cycle life.

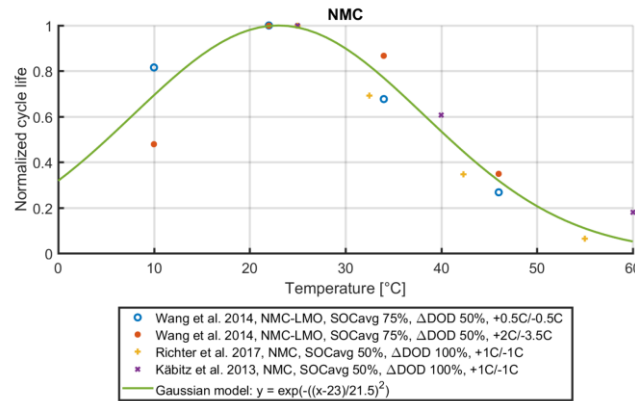


Figure 8: Aging stress factor related to temperature [7].

The temperature stress factor is normalized according to the room temperature and the fitted equation representing the temperature factor is found as below [7]:

$$nCL(T) = e^{-\left(\frac{T-23}{21.5}\right)^2}$$

Equation 5 Temperature stress factor.

4.1.3.3 Average State-of-Charge (SOCavg)

The aging stress factor related to SOC_{avg} for NMC cell is developed in [7]. Figure 9 depicts the experimental results and fitted equation.

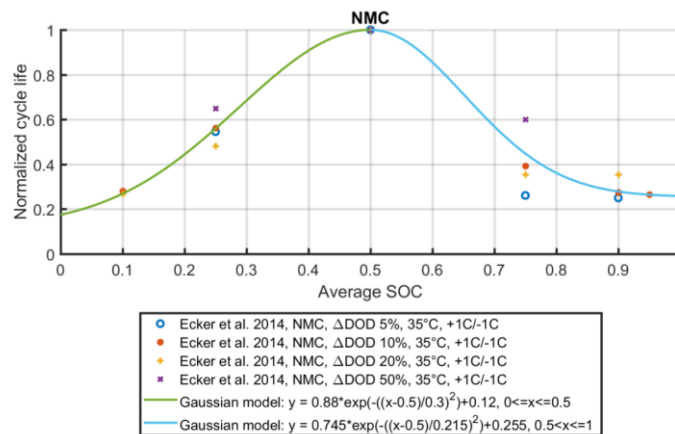


Figure 9 Aging stress factor related to SOC_{avg}.

As seen in Figure 9, an exponential curve is found in which the highest life cycle is achieved at SOC_{avg}=50%, and the stress factor can be formulated as:

$$nCL(SOC_{ave}) = \begin{cases} 0.88e^{-\left(\frac{SOC_{ave}-0.5}{0.3}\right)^2}+0.12, & 0 \leq SOC_{ave} \leq 0.5 \\ 0.745e^{-\left(\frac{SOC_{ave}-0.5}{0.215}\right)^2}+0.255, & 0.5 \leq SOC_{ave} \leq 1 \end{cases}$$

Equation 6 SOC stress factor.

4.1.3.4 C-rate

To model the impact of C-rate on cycle aging, the experimental results of Burzyński [8] is used. The cycle aging tests for the NMC battery done at 25 degC for 100% DOD at different discharge C-rates. However, we assume an identical impact for charge C-rate, therefore the C-rate stress factor will be used for both charge and discharge processes.

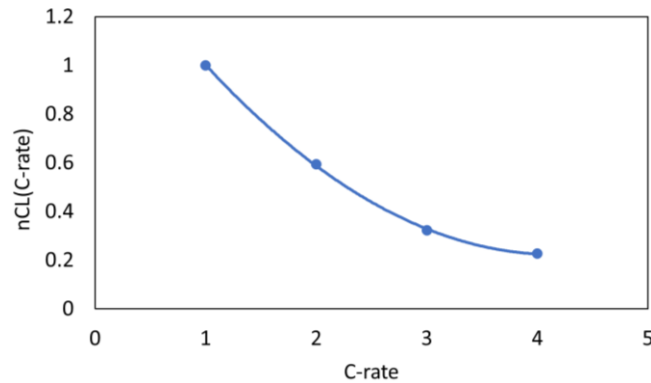


Figure 10 Aging stress factor related to C-rate.

The stress factor related to C-rate can be formulated as a polynomial equation given below:

$$nCL(C - rate) = 0.0778 \times (C - rate)^2 - 0.6478(C - rate) + 1.5722$$

Equation 7 C-rate stress factor.

Although the presented cycle life estimation model considers four aging parameters, for HYPOBATT digital twin model only the impact of Temperature and C-rate are the important factors as the digital twin model aims to optimize the charging of the battery. Therefore, in the next steps the presented model has to be adapted to HYPOBATT application by excluding DoD and SOCavg impact.

The impact of C-rate and temperature are given in mathematical equations separately. On the other hand, the temperature of the battery depends on the C-rate. Accordingly, an optimization algorithm for charging has to optimize the impact of temperature and C-rate on aging based on the given aging equations, while providing proper charging profile for the vessel.

4.1.4 Safety considerations

The current standard for battery safety is focused on temperature and voltage, since these are the two most accessible parameters sensing wise. Having these, boundaries for both are defined according to the specifications of the battery system manufacturer. Parameter definition regarding temperature range will be further optimized with the aging model of the battery.

IEC 62619 specifies requirements and tests for the safe operation of secondary lithium cells and batteries used in industrial applications including stationary applications. In the current application the following aspects need to be considered:

4.1.4.1 Temperature/voltage/current management

The design of batteries shall be such that abnormal temperature-rise conditions are prevented. Battery systems shall be designed within voltage, current, and temperature limits specified by the cell manufacturer. Battery systems shall be provided with specifications and charging instructions for equipment manufacturers so that associated chargers are designed to maintain charging within the voltage, current and temperature limits specified.

4.1.4.2 Battery system design

The voltage control function of the battery system design shall ensure that the voltage of each cell or cell block shall not exceed the upper limit of the charging voltage specified by the manufacturer of the cells, except in the case where the stationary application devices or motive application devices provide an equivalent voltage control function.

The following should be considered at the battery system level and by the battery manufacturer: For the battery system which has series-connected plural single cells, modules or battery packs, it is recommended that the voltages of any one of the single cells or cell blocks do not exceed the upper limit of the charging voltage, specified by the cell manufacturer, by monitoring the voltage of every single cell or cell block. The BMS is the electronic system associated with a battery which has functions to cut off in case of overcharge, overcurrent, overdischarge, and overheating.

Having the above information provided, overvoltage, overheating and overcurrent will be monitored and taken into account to manage charging profiles latter on in the project.

4.1.5 Connection setup to the charger

2 main connections are done, with the 2 DC terminals. Charger receives information regarding the battery voltage state for the thermal losses calculation and the amount of charging it will provide. Charging control will be done outside the DT, so no further communication between the batteries and the charger model is established.

4.2 Vessel MW Charger Models – Transformer

The transformer is a three-phase three-winding transformer composed of a Delta primary, and two Wye secondary windings, around a three-limb core. In practical applications, the low-voltage side windings should be grounded through a resistance or reactance to limit earth fault currents. This connection type is usually used in double secondary transformers, which means that both low-voltage windings are identical.

The transformer modelling is composed of an electrical model, where the electromagnetic behaviour is represented and from which the power losses are measured and a thermal model in which the temperature increase is obtained.

4.2.1 Transformer electrical model

The model of a three-phase three-winding D-Y-Y transformer is similar to that of a single-phase three-winding transformer. A single-phase three-winding transformer can be modelled as shown in Figure 11.

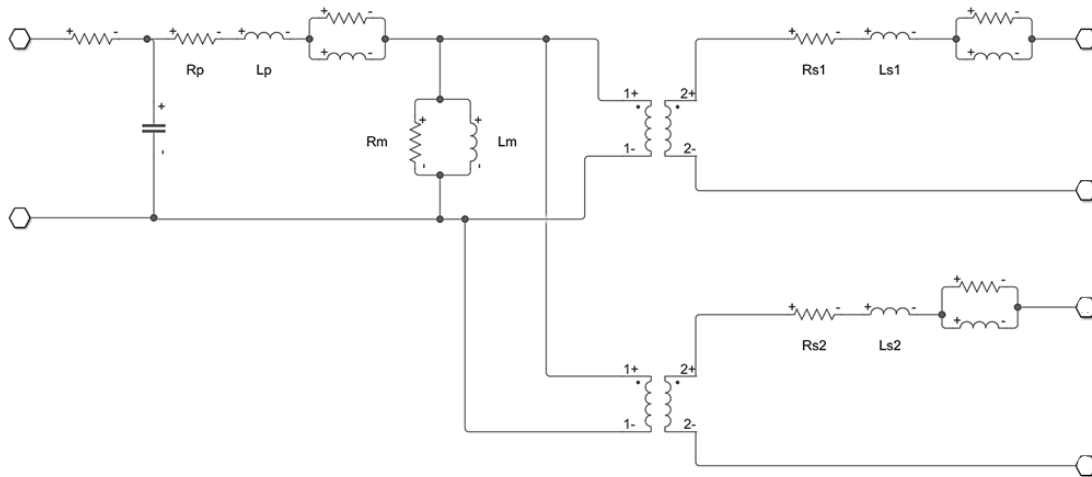


Figure 11 Single phased three windings transformer electrical model

The model includes the equivalent leakage impedance of the three windings, and a magnetizing branch for modelling the core losses, as well as an ideal transformation ratio. This model is reasonably accurate when the core is not saturated and is the most used in power systems studies. If a more accurate behaviour of the magnetic core is required, there are another equivalent circuit models, such as the proposed in [9] where it is possible to get very accurate results when the model is used to describe the behaviour of the magnetic core, adding the saturation curves instead of the typical nonlinear resistance model.

Besides including all the parameters explained to adequate the single-phase model to the three-phased one, it is important to take into account the zero-sequence impedance. The equivalent circuit of this impedance depends on the type of winding connections and the core construction. The different zero sequence impedance circuits for various winding configurations are well described in [9].

As the transformer is connected to the grid, a frequential model is implemented using the foster equivalent impedance to support the incoming harmonics. This equivalent circuit is useful for analysing the frequency response of a transformer, as it allows the prediction of the transformer's behaviour under different operating conditions, such as frequency and load variations. The circuit is composed by a combination of series and parallel impedances that represents the winding resistance and leakage inductance for different frequencies. It is important to emphasise the importance of using this approach in the model, since the harmonics coming from the grid can have a big impact and it is crucial to take them into account.



It is also important to include an equivalent parasitic capacitance in the input of the system, considering the winding to winding, layer to layer and the stray capacitance in order to be able to measure and detect possible resonances in the circuit.

In order to create the electrical model, the data in Table 3 must be known.

Table 3 Transformer parameters needed from the manufacturer for the electrical model.

Transformer Parameters
Winding Voltages (primary, secondary, ...)
Number of turns N
Connexion type Δ - Yy - Yy
Leakage and magnetizing impedance $L_p, R_p, L_s, R_s, L_m, R_m$
Zero-sequence impedance L_0, R_0
Winding capacitance C_1

As it can be seen on Table 3, some test must be done to the transformer in order to obtain the necessary data. On the one hand, the no-load loss test measures no-load losses at a specified excitation voltage and frequency, more details can be found in [10]. On the other hand, the load loss test determines not only the losses in the transformer under load, but also the impedance of the unit. Finally, the zero-phase sequence test measures the zero-sequence impedance at a rated frequency between line terminals.

Using this model, the primary and secondary windings losses and the core losses are measured from the circuit. These losses are used in the thermal model for estimating the temperature increase of the transformer.

4.2.2 Thermal model

For modelling the thermal behaviour of the transformer, a thermal network is used. A thermal network is a mathematical model that represents the thermal behaviour of the transformer by means of an electrical circuit. The model is used to predict the temperature rise under different operating conditions, such as load and ambient temperature variations. These networks include several thermal resistances that represents the heat transfer between the different parts of the transformers.

The transformer resistance network can be divided into three main components: conduction, convection, and radiation.

4.2.2.1 Conduction

The conduction resistance is divided in the air conduction resistances and the conduction resistances in a solid body.

Air conduction resistance in natural convection refers to the resistance to heat transfer that arises due to the conduction of heat through the air. The air conduction resistance is a function of the thermal conductivity of the air, the air density, and the distance through which heat is conducted. It is calculated using *Equation 8*. These resistances are used when no moving air is considered in that area.

$$R_{conduction} = \frac{d}{k A}$$

Equation 8 Conduction resistance

Where d is the distance over which heat is conducted, k is the thermal conductivity of the air, and A is the cross-sectional area of the air flow.

The conduction resistance in a solid body is determined by solid components, such as the windings and the core, and the thickness and area of each component. The same *Equation 8* is used for calculating this resistance, where d is the thickness of the component, k the thermal conductivity of the component and A the component cross-sectional area.

4.2.2.2 Convection

The convection resistance is determined by the coefficient of heat transfer between the transformer's surface and the surrounding air, and the area of the surface *Equation 9*.

$$R_{convection} = \frac{1}{h A}$$

Equation 9 Convection resistance

Where h is the heat transfer coefficient and A is the surface area.

The heat transfer coefficient is a function of several factors, including the temperature, density, volumetric expansion coefficient, dynamic viscosity, kinetic viscosity, and thermal conductivity.

Once the mentioned parameters are obtained for each node, the different correlations equations are applied for calculating the h . In this case, the nodes that involve convection are in laminar regime and natural convection, so the heat transfer coefficient is calculated using the Nusselt correlation equation divided in the vertical and horizontal direction *Equation 10*.

$$h = \frac{Nu k}{L}$$

Equation 10 Heat transfer coefficient equation

Where Nu is the Nusselt number for vertical or horizontal direction, k is the thermal conductivity and L is the characteristic length in vertical or horizontal direction.

The Nusselt number is a dimensionless number that describes the ratio of convective heat transfer to conductive heat transfer in a fluid. It can be calculated analytically, based on the Grashof number (Gr) and the Prandtl number (Pr). In the Table 4, the Nusselt number analytical equations for horizontal and vertical orientations are shown.

Table 4 Nusselt number analytical equations.

Nu horizontal	$Nu = 0.54 (Gr Pr)^{\frac{1}{4}}$
Nu vertical	$Nu = 0.59 (Gr Pr)^{\frac{1}{4}}$

The Grashof number is obtained from Equation 11.

$$Gr = g \beta L^3 \frac{\Delta T}{\nu^2}$$

Equation 11 Grashof number equation

Where g is the acceleration due to gravity, β is the coefficient of thermal expansion, ΔT is the temperature difference between the surface and the ambient, L is the characteristic length and ν is the kinetic viscosity. This number is calculated for horizontal and vertical areas.

The Prandtl number is obtained from Equation 12.

$$Pr = \frac{k}{c_p \nu}$$

Equation 12 Prandtl number equation

Where k is the thermal conductivity, c_p is the specific heat capacity and ν is the kinetic viscosity.

It is important to mention that this Nusselt approximation equation is only accurate for laminar flow regimes, it is not suitable for turbulent regimes. Additionally, this equation is based on a general assumption, and it may not be accurate for some specific cases, such as low Grashof number and high Prandtl number. Another manner for calculating this is using the Churchill-Chu correlation approach which is explained in [11].

4.2.2.3 Radiation

The radiation resistance is determined by the coefficient of heat transfer between the transformer's surface and the surrounding surfaces, and the area of the surface. Equation 13 is used for calculating this resistance.

$$R_{radiation} = \frac{1}{\sigma e A \Delta T^4}$$

Equation 13 Radiation resistance equation

Where e is the surface emissivity, σ is the Stefan-Boltzmann constant, A is the area of the surface and ΔT represent the temperature difference.

In the case of the three-phased three-winding transformer, the implemented thermal network has several nodes all over the transformer core and windings. The connection between different nodes has been performed by adding resistances that model conduction, convection and radiation heat exchange as previously explained.

As in the electrical model, in order to be able to model the transformer thermally, some parameters must be given by the manufacturer. These parameters are the transformer core and winding dimensions, and the core losses and winding losses curves with respect to the temperature.

4.2.3 Implementation and safety considerations

This model has been implemented in Simulink software, by means of electrical and thermal blocks available on Simscape library. The connection between the electrical and thermal model is done using the core and windings nodes, where the losses obtained from the electrical model are divided between the mentioned windings and core sections and inserted as a thermal energy source.

Regarding the transformer safety aspect, one of the most common issues in this type of transformers is the tank vibration, that is able to change the mechanical properties of the core and windings. An accelerometer and other vibration analysis equipment can be used to monitor the transformer's core, shield, and moving elements from the outside. The most common mechanical damages (such as looseness, misalignment, unbalance, and other issues) can be detected and tracked using vibration analysers [12] [13].

In this case, as the transformer does not have any sensor, the safety aspect has been focused on controlling the temperature rise monitored by the thermal model, with the possibility of including an alarm if the temperature exceeds a predetermined value. This is one of the key points of the transformer model in the digital twin, as it is not necessary to include temperature sensors in the physical transformer for measuring the temperature gradient at joints and other exposed areas.

4.3 Vessel MW Charger Models - Converter

The charger converter model is composed of two domains, the electrical domain in which no power losses are calculated and the thermal domain where the power losses are calculated to estimate the converter inner temperature. The thermal model is dependant of the electric one, as the data collected from this last domain is used to calculate the converter losses.

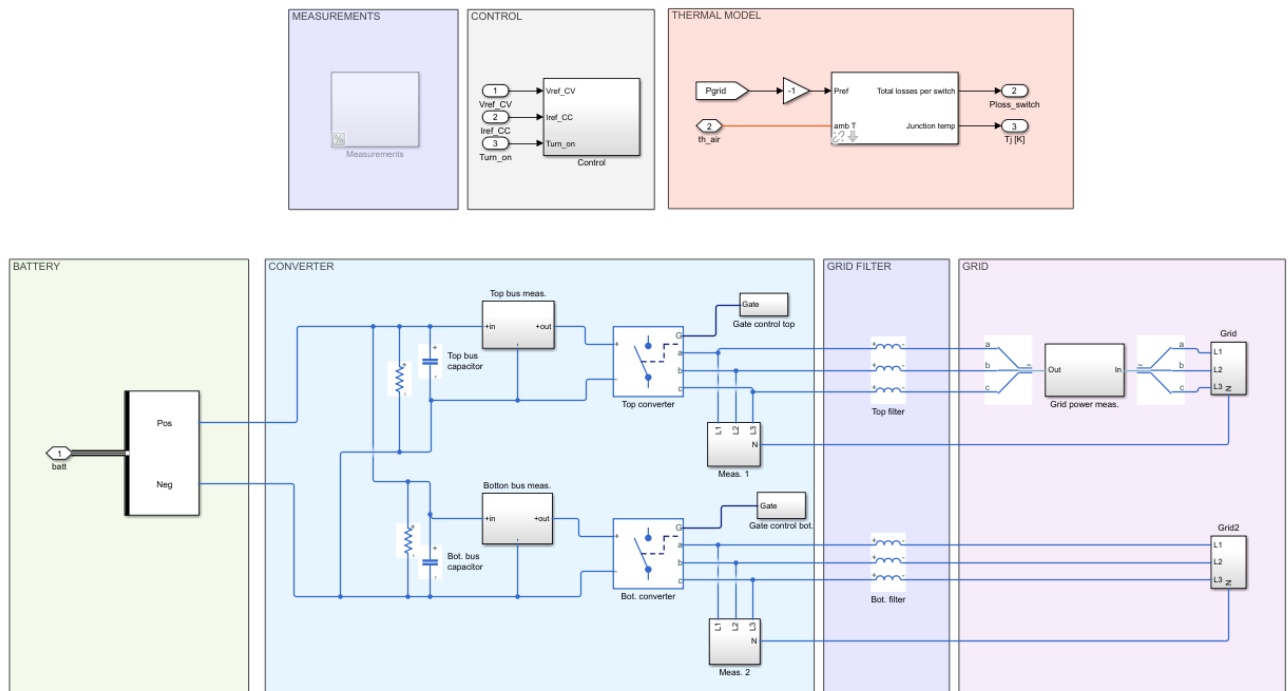


Figure 12: General view of the converter model.

To develop the two models, the following simplifications were done:

- In the electric model no losses are considered (ideal converter).
- The two converters are considered identical, the thermal model is simplified to one.

4.3.1 Major components data for initial modelling

For the electric domain, the battery flotation voltage setpoint, maximum charging current setpoint and grid voltage sensing are necessary to perform the simulation. A typical CC/CV battery charging profile can therefore be performed.

On the other hand, for the thermal calculation the datasheet parameters of the converter's switches (Forward voltage ($V_{ce,th}$), Ohmic voltage drop ($R_{ce,on}$), thermal resistance (R_{th}), ...) and the ambient temperature inputs are necessary. Additionally, information about the employed cooler is necessary. Initial parameter values have been used, with the possibility to use the real component parameters after the final design is completed.

4.3.1.1 Topology

The topology of the converter is shown in Figure 13. The AC/DC is composed of two series or parallel connected AC/DC converters. Depending on the battery voltage level a series-connected or parallel-connected topology is more suitable. For a low voltage battery (i.e. 500V to 1000V) with higher currents, a parallel connection is more suitable to alleviate current stress in the converters. Conversely, for a high-voltage battery (i.e. 1000V ... 2000V) a series connection is more suitable to alleviate voltage stress in the converters.

Having in mind that the most likely battery voltage will have a voltage range of 800 V to 1 kV the parallel connection is the most suitable converter topology for the application.

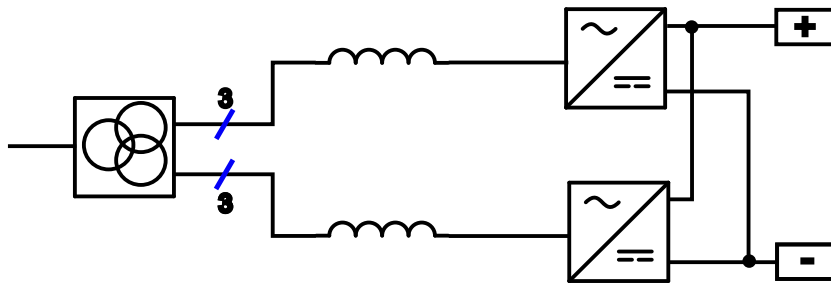


Figure 13 Corner-ground mid-point two parallel connected AC/DC rectifiers.

4.3.1.2 Electro-Thermal model

The electrical model is a no current control loop average model, no commutations are simulated and the synchronization between the grid and converter is achieved by equations, considerably reducing the simulation time. This model receives as an input the battery voltage provided by the battery and the constant current and voltage values set by the operator with which the converter performs a typical charge profile:

1. Constant Current charge (CC): The battery is charged with a specified constant current until the battery reaches a pre-set voltage level and the constant voltage charge begins. The current reference can be changed during charging.
2. Constant Voltage charge (CV): A constant voltage is applied to the battery, for this reason, the current reduces as the battery becomes fully charged.

The thermal model is based on Cauer thermal network, Figure 14. The first node represents the junction of one of the semiconductors of the converter and it is connected to the heatsink node by some thermal resistances; in the heatsink node the rest of the converters switch nodes are gathered and a convective connection with the ambient is done. The source of heat of each switch is calculated by analytical equations; these equations, based on values obtained from the switches' datasheets, converter current intensity, phase delay and bus voltage, are fast and relatively accurate.

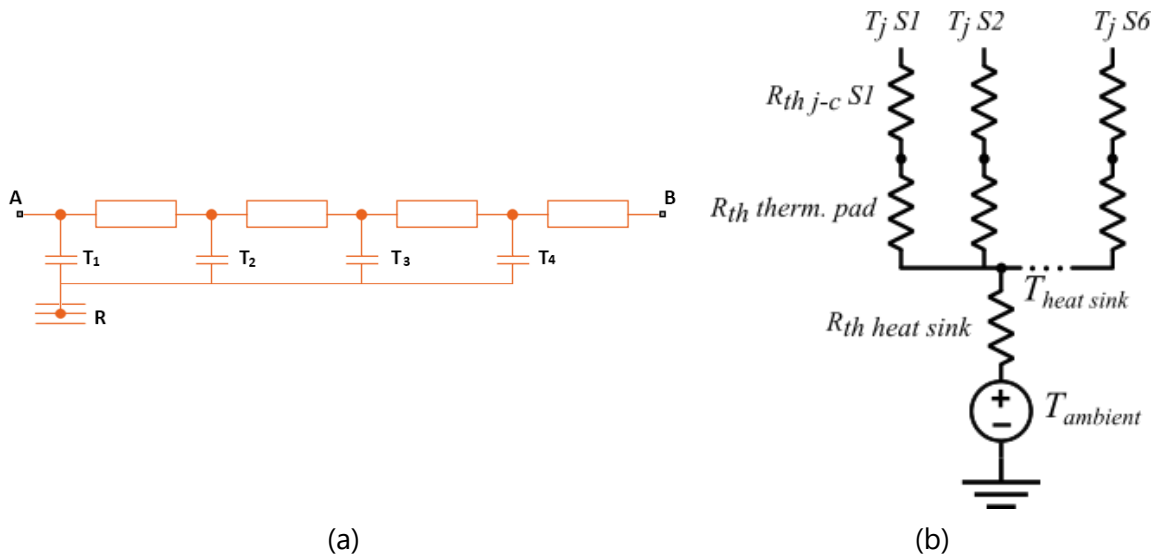


Figure 14: Thermal model: (a) Cauer model [14], (b) converter model's equivalent thermal circuit.

The developed model has been tested with the above explained charging profile to perform a unit testing. The obtained different waveforms from the simulation can be seen below.

In Figure 15 the applied charge profile can be seen, where the battery is charged with 75A constant current where the battery is first charged with a constant current of 1 kA until the current reference is changed to 1,5 kA. On the other side, in Figure 16 it is shown the grid current waveforms when the charging of the battery begins. The converter starts to incrementally consume power, rising the current intensity of the grid. Finally, in Figure 17 the converters switch junction temperature evolution can be seen.

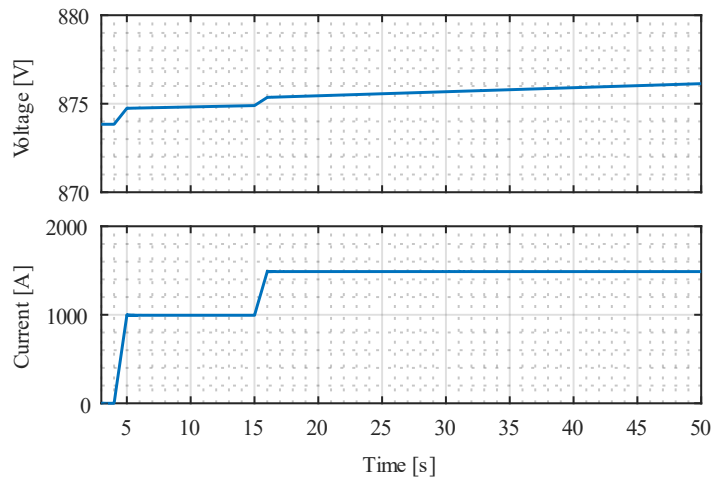


Figure 15 Battery voltage and current waveforms during charging (unit test).

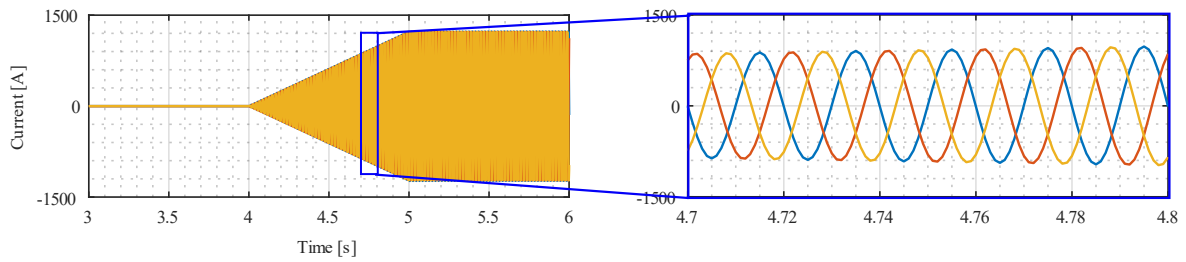


Figure 16 Grid current waveforms at the beginning of the charging.

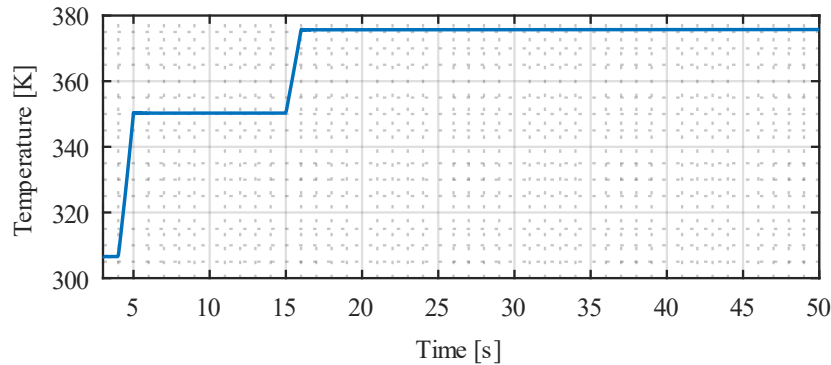


Figure 17 Converter switches junction temperature.

To achieve a fast electro-thermal converter model, several iterations over the first electro-thermal model have been necessary, shown in Figure 18.

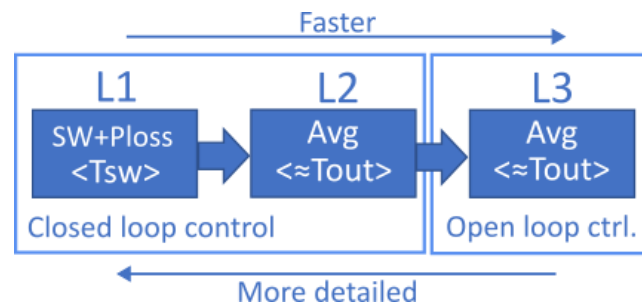


Figure 18 The generated different model levels; <Averaging window width>.

The first built model was a switched model, that is, every commutation of each switch was simulated. Besides, in each commutation moment the voltage, current and junction temperature (T_j) values were used by the thermal domain to calculate the commutation power losses of the semiconductors, which made the overall simulation even more complex. Due to the complexity, the computational load of the simulation was huge, requiring a simplification of the model. To solve this, a new average model was built. In the electrical domain the commutated switches were replaced by averaged semiconductors. In the thermal domain instead, analytical equations were included to calculate the power losses.

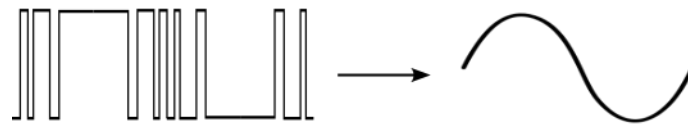


Figure 19 Output voltage waveform example of a switched converter leg (left) and an average converter (right).

This ignores fast-dynamics information, but retains only close to grid-frequency information, to accelerate the simulation time.

Due to these changes, the simulation time was notably reduced, however, it remained quite big. This time, the current loop control was removed. Although this made the simulation faster, the following simplifications had to be taken:

- Grid voltage frequency and amplitude are invariant.
- The grid's initial condition must be specified so that the converter and the grid are synchronized.
- Grid's voltage phase delay is not current-dependent.

Due to these simplifications, as the transformer injects a phase-delay on the voltage that makes the converter synchronization with the grid impossible without a current control loop. It was necessary to electrically de-couple the transformer and converter models. Although the two model are separated, the transformer is dependant of the converter model, achieving the same current intensity and, therefore, the same power in both sides, conserving the thermal domain accuracy while achieving a fast simulation time.

4.3.2 Charger inputs and outputs

The charger will be connected to the grid to receive the available power from the grid. This will be fundamental in establishing the proper charging profile. Power losses and temperature hotspots will be essential to monitor and enhance the charger efficiency. The final charging power will be also the further output to the battery model, present in Figure 20.

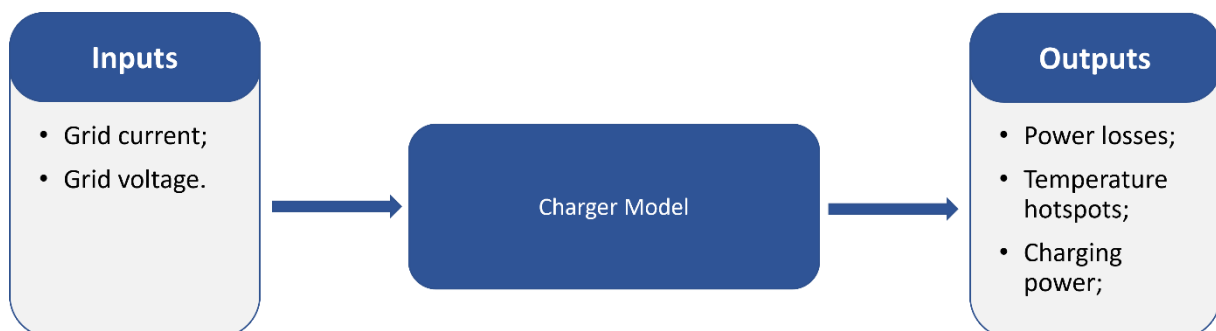


Figure 20 Charger model inputs and outputs.

4.3.3 Safety considerations

For the safe activity of the converter the following considerations are normally taken into account:

- Under Voltage (UV): This element avoids the connection of the converter to the grid if the bus voltage is too low, as if the voltage drops below a specific level, the converter becomes control less.
- Over Voltage (OV): Prevents the bus voltage exceeding its limits.
- Over current (OC): This protection confines the current flow to a safe level.
- Power derating: The derating curve indicates the maximum specifications according to different parameters as temperature, output current/voltage, commutation frequency, etc. which ensures the device is working in safe conditions.

These values and other more specific values are to be confirmed in WP3.

5. VESSEL MW CHARGER MODELS – SCALABILITY & OPTIMIZATION

5.1.1 Scalability towards multiple transformers & converters

The charger model contains both the transformer and converter as described in chapters 4.2 and 4.3. To make the model scalable, the number of chargers and transformers, operating in parallel should be adaptable. Therefore, the addition was made to the model with the following assumption: that all converters and transformers share the load equally and operate identically. This assumption makes it possible to only simulate a single instance of the models and to not negatively impact the overall simulation speed. In the new model, the number of converters and the number of transformers can be varied independently as two distinct parameters.

5.1.2 Optimization speed towards large scale simulation

For larger scale simulations for e.g. hourly and daily planning operations, but also for real-time digital twin simulations, the simulation speed can be increased by applying additional assumptions in the model. Multiple ways of speeding up the model were tested, and an overview is provided in Table 5.

Table 5 Speed optimization towards large scale simulation

Adjustment to the charger model	Impact on the simulation speed
Replace the converter blocks by ideal current sources	~2 times faster
Ignore parasitic components of the transformer in the electrical simulation	~2.5 times faster
Increase the simulation time step size	Significant
Simplify the thermal model of the transformer	Negligible

5.1.2.1 Replace the converter blocks by current sources

In the detailed model, two three-phase converters and filtering inductors are used as an interface between the AC grid and the DC battery. These converters require a control system for generating the correct gate signals. A simplification with minimal accuracy loss can be made by replacing the converter blocks by current sources.

The current of the current sources is determined in each simulation step by dividing the power reference by the voltage of the battery. The power reference originates from the Voltage PI loop in the control block. The current control is passed through the transfer function of a first order low-pass filter to avoid abrupt changes in current, overshooting and ringing.

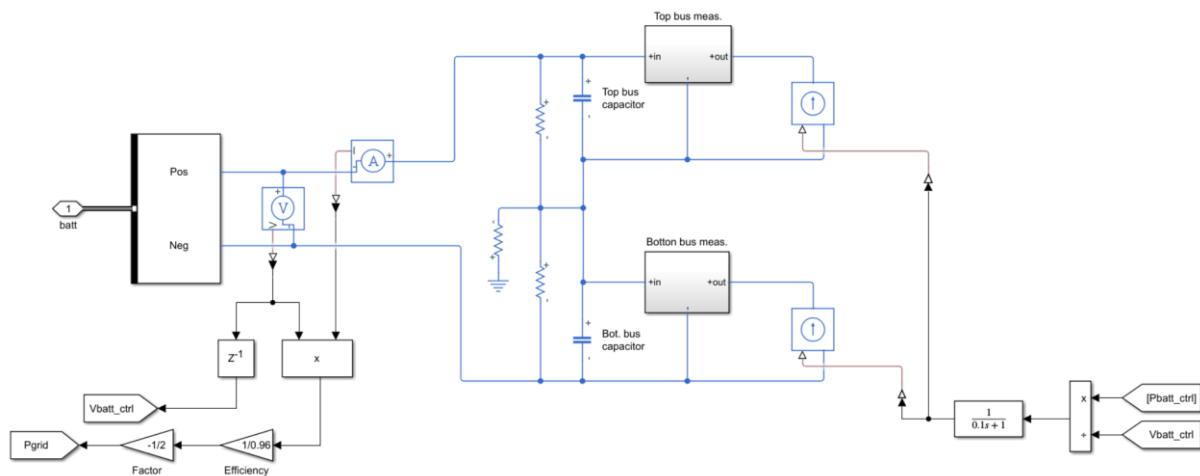


Figure 21: Converter operation by ideal current sources

5.1.2.2 Ignore parasitic components of the transformer in the electrical simulation

The simulation model of the transformer contains a significant number of resistors and inductors that represent the winding and core losses and leakage and magnetizing components of the transformer.

As these passive components have a limited influence on the control and actual currents running through the transformer windings, a simplification can be made to the model by removing them. A slight drop in accuracy will occur and possible resonances can not be detected anymore, this is a trade-off between accuracy and simulation speed.

5.1.2.3 Increase the simulation time step size

Simulation time step size refers to the amount of time that is simulated during each iteration of the model. If the step size is increased, the model will simulate larger time intervals per iteration, which means that fewer iterations will be needed to simulate the same overall time period. This reduction in the number of iterations can lead to a significant increase in simulation speed. However, increasing the step size too much can also lead to inaccuracies in the simulation results. Therefore, it is important to carefully consider the appropriate step size based on the specific simulation model and the desired level of accuracy.

The highest frequency present in the model is the frequency of the grid. According to the Nyquist theorem, the maximum frequency that can be accurately represented in a sampled signal is half the sampling frequency. This means that the simulation time step size should be at least two times larger than the inverse of the grid frequency.

The simulation time step size can be increased even further if losses in the model are calculated with averaged values, this is possible as long as the grid is considered as a constant voltage source with a stable frequency.

5.1.2.4 Realised optimisations

Without the simplifications implemented, simulating 120 seconds takes 6 minutes. This is reduced to only 48 seconds by removing the converter blocks and parasitic components of the transformer model as described above.

Table 6 Simulation times with described speed optimizations

	Simulation time	Real Time
Original model	120 seconds	360 seconds
Adjusted model	120 seconds	48 seconds

Figure 22 shows simulation results of the battery voltage and current for both the original model and the adjusted model. Both simulation results overlap with only little differences. The models only differentiate at sudden current transitions, where the detailed model shows ringing and overshoot, this is not the case for the adjusted model. Important to note that these values do not represent the final response of the DT as it is built upon non representative variables.

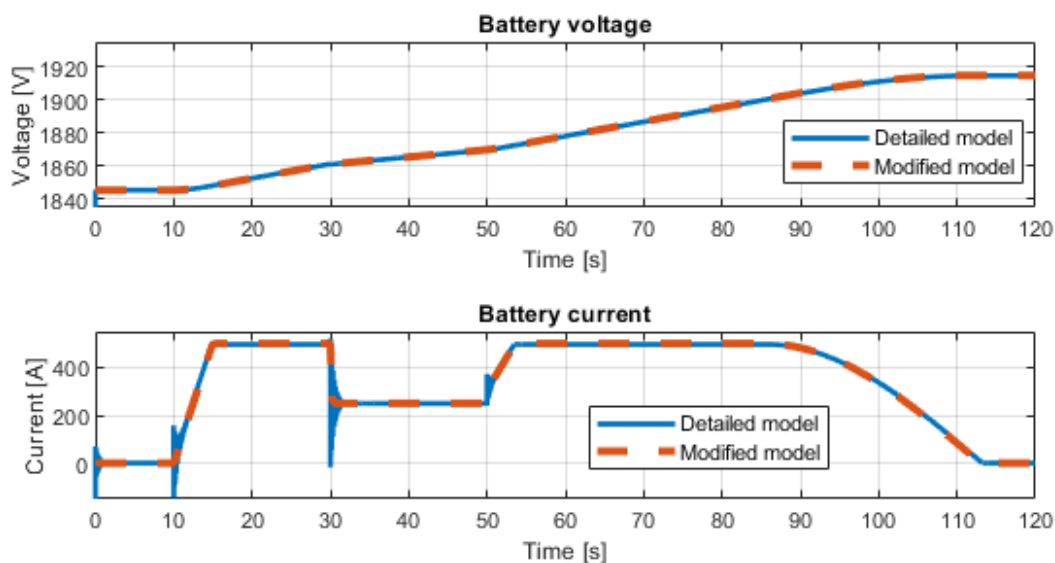


Figure 22: Battery voltage and current with the speed optimized model

Figure 23 shows simulation results of the losses originating from the three-phase converter. It is split up in the conduction losses of the switch, conduction losses of the diode and, largest of all, the switching losses themselves. It is clear that the accuracy of the model is very high, except for the setpoint transitions where the fastest dynamics are not included in the simulation.

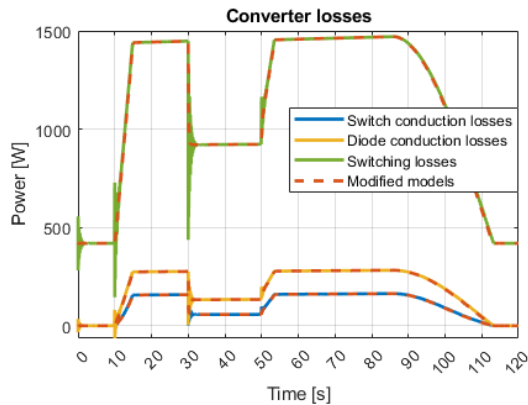


Figure 23: Converter losses with the speed optimized model

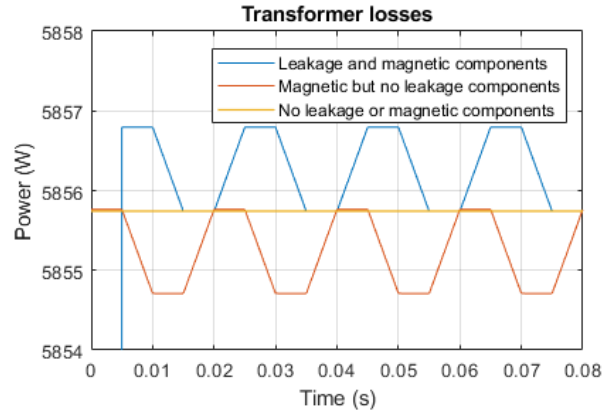


Figure 24: Transformer losses with the speed optimized model

Removing the leakage and magnetising components from the transformer model introduces a small phase shift on the output voltage of the transformer. The losses related to the transformer change slightly when the magnetic and leakage components are removed. However, the speed increase from neglecting the electrical effect of these components is significant as indicated by Table 7.

Table 7 Simulation times when optimizing the electrical/magnetic transformer model

	Simulation time	Real Time
Both leakage and magnetic components	120 seconds	220 seconds
Only magnetic components	120 seconds	85 seconds
No leakage or magnetic components	120 seconds	80 seconds

The losses in the windings and in the transformer core, however, are still being calculated. Figure 24 shows simulation results for the losses of the transformer model with leakage and magnetic components, with magnetic components but without leakage components and without both leakage and magnetic components. Note the limited range of the vertical scale, the magnetic and leakage components have very little influence on the magnitude of the transformer losses.

5.2 Grid Model

The integration of vessel charging station, photovoltaic (PV) production and future electrical vehicle (VE) charging infrastructure in parking involves modifications in the Norddeich port's

power grid configuration. As these modifications have been carried progressively, modelling of power grid will take into account successively this multistep evolution, in providing various model versions. The main objective is to study the digital twin system combining grid model, vessel charger and battery in different situations. Grid model will be declined under three versions:

- Model 1: grid model as existing system including consumption load (building...), with addition of new feeder allowing the connection of the vessel charger.
- Model 2: a PV system and EV charging loads are added to the grid's model 1. In this version, PV system is modelled as a current supply, and EV charging load as constant power loads, meaning that high dynamic transient and protection event related to these elements are not considered.
- Model 3: This model uses the same configuration as model 2, with differences in PV system model and EV charging loads model. The latter include model behaviour in case of transient phenomena such as grid frequency and voltage variation. With this consideration, digital twin will be able to consider the global operation of port's power system during dynamic transient.

Power grid system is modelled and parameterized with data provided by Frisia. Some parameters could not be collected so arbitrary data or commercial datasheet have been used.

5.2.1 Architecture and evolution

The current architecture is established as follows:

- One line simplified electrical diagram of power grid structure in the Norddeich port is shown in the Figure 25. Main elements described in this grid are: Public grid connection at 20kV.
- Existing port's loads such as building and ancillary consumptions
- Lines to connect existing part to the new part which are: 420m vessel charger feeder which is connected to the charger converter; 590m feeder to connect two PV installations and EV charging infrastructure.
- A transformer 0.4/20kV between 20kV and 400V grid area, which has a 2.5MVA nominal power.
- As explained previously, EV charging load and PV production are integrated in a second phase, hence, they are included in model 2 and model 3.

As vessel battery and charger are specific models, grid model does not cover these elements in its scope.

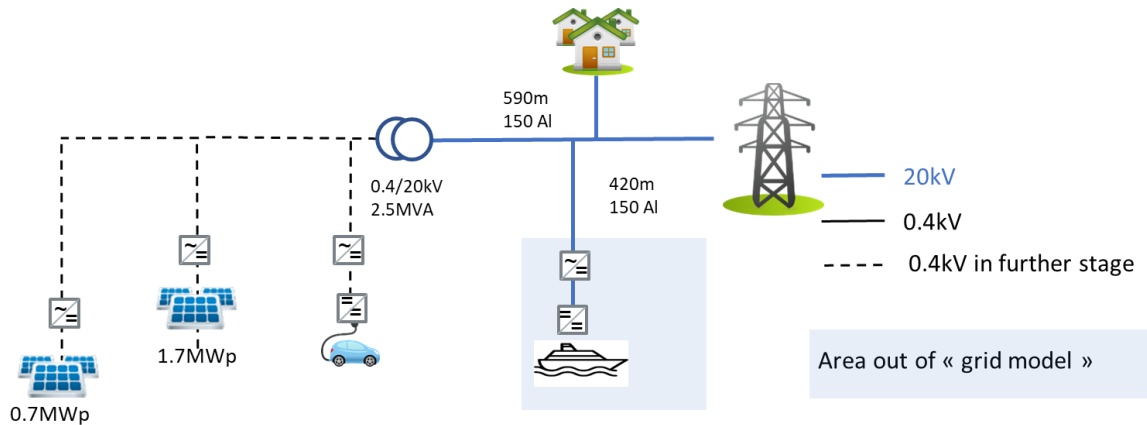


Figure 25 Electrical diagram in Norddeich port.

Grid model is mainly built using MATLAB Simulink/Simscape library components. In the following session, each component model is described, with assumptions related to model parameter setting. Grid model is illustrated in Figure 26.

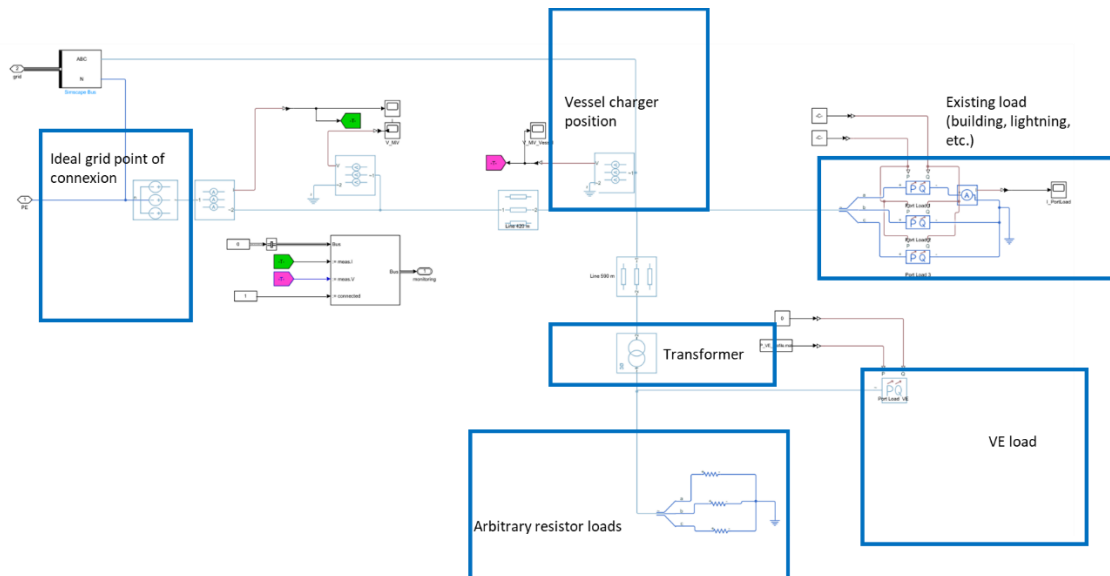


Figure 26 Model of Norddeich port power grid with Simscape.

5.2.2 Component models

5.2.2.1 Public grid connection

The connection between the port's power system and public grid is represented by a three-phase voltage source. The modelling assumes hypothesis of ideal voltage signals supply from the grid with nominal voltage and frequency, which are respectively 20kV and 50Hz. Furthermore, unlimited power exchange is considered between the port's grid and the main grid based on the hypothesis of port power system's oversizing. In Figure 27, main grid connection model and parameters are illustrated.

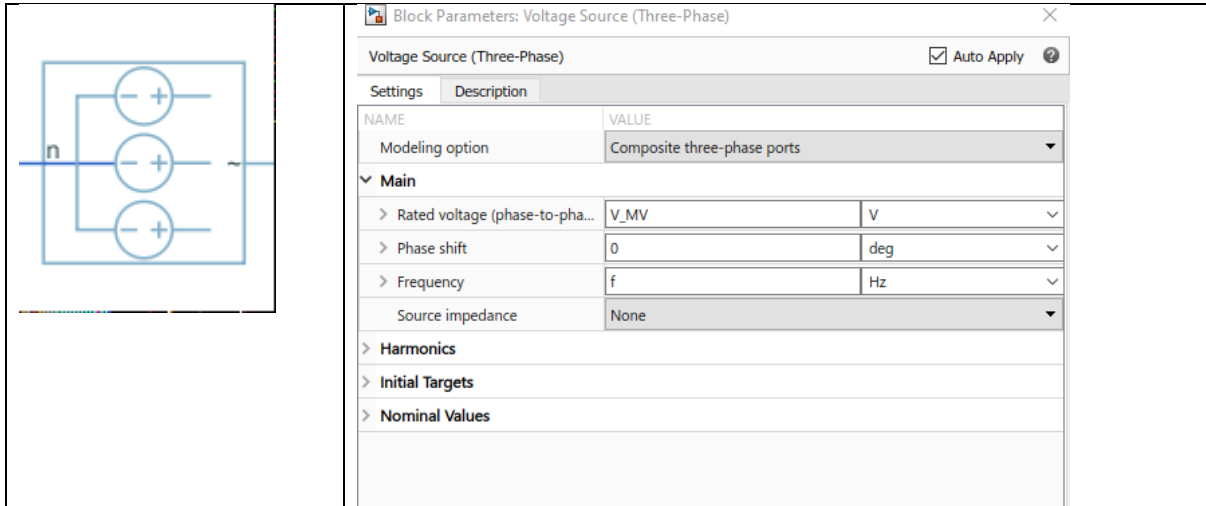


Figure 27 Model of public grid connection.

5.2.2.2 Lines

Based on port electrical diagram, lines modelling can be performed using their parameters such as length and cable model. Simscape RLC three-phase impedance model are employed. Impedance parameters such as cable resistance and inductance are computed based on cable datasheet [15] and expert data.

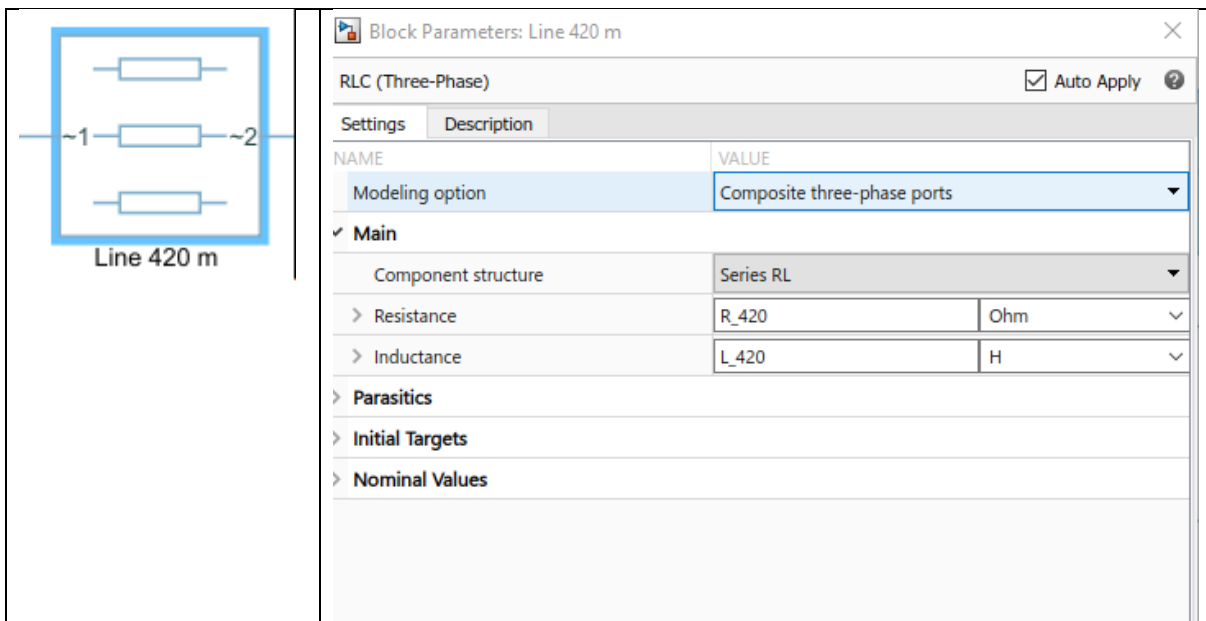


Figure 28 Model of the line.

5.2.2.3 PV

Two PV plants have been planned for installation in the port area, in order to partially cover port's consumption. PV system construction will be in two steps, with a 1.7MWp production plant for the first phase and an additional 0.7MWp plant in the second phase.

There are two options to consider PV system modelling:

- PV system is simply modelled as a variable AC current source. In this option, PV plant provides variable current or power to the port system, which is described by a time series input vector that represents time variable irradiation. In this option, PV inverter behaviour is considered as unchanged related to grid's signal.
- This option considers PV system inverter behaviour according to grid's state, such as frequency and voltage operation ranks and Fault Ride Through (FRT) capability. Frequency and voltage rank characteristics are generally defined by inverter manufacture specification as in the example of industrial PV inverter [16]. Accurate values of F_{min} , F_{max} , V_{min} and V_{max} , which are respectively inverter's operating maximum/minimum frequency and voltage can vary according to each country grid codes. Out of these ranks, PV inverter disconnects from the power system and stop providing its production. A delay duration T_s is given for fault detection and active the inverter disconnection. Parameters of operation rank and FRT parameters used in our actual model are summarized in Table 8.

Table 8 PV parameters.

PV Parameters	Value and Unit
Nominal frequency, f	50 Hz
Minimum frequency, F_{min}	44 Hz
Maximum frequency, F_{max}	55 Hz
Nominal voltage (phase to phase), V_{LV}	230 V
Minimum voltage, V_{min}	0.9 V
Maximum voltage, V_{max}	1.1 V
Delay to reconnection after a fault, T_s	5 s

- On the other hand, FRT capacity can be required as PV inverter feature aiming to help grid's stability maintaining. Indeed, in order to avoid cascade production power losses following a disturbance that have led to voltage drops, some grid codes have been released to require PV plant to maintain connected their production during certain time laps which is various according to grid voltage drop during the disturbance. This expected behaviour is different from a country to another. Some examples are illustrated in Figure 29. Germany and Italy grid codes are of the stricter as they require PV production to stay connected even when voltage sags are complete (grid voltage at the Point of Common Coupling is 0).

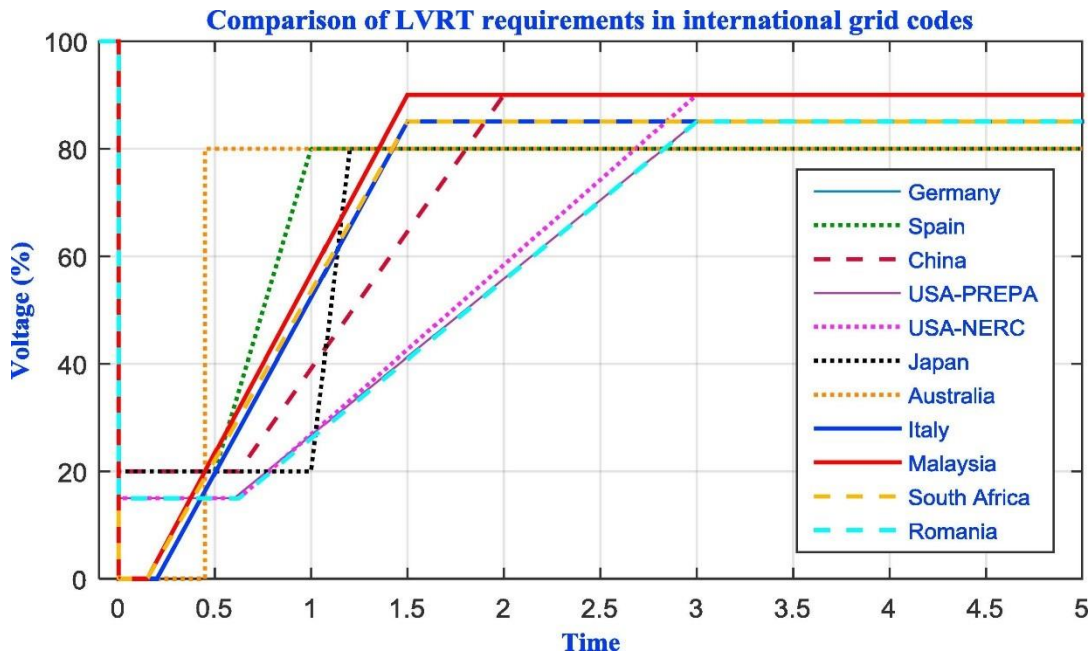


Figure 29 Example of FRT grid codes. Adapted from [17].

5.2.2.4 Transformer

As illustrated in Figure 25, PV installation output voltage is 400 V, which is Low Voltage (LV). An internal substation is built to deal with the PV system connection to the grid lines, where the voltage is 20kV (Medium Voltage- MV). The substation equipment includes devices for control and protection of the coupling point. The main device is a 400V/20kV transformer, which deals with voltage transforming. Only the transformer is modelled to represent the substation, as seen in Figure 26. A standard two-winding transformer model from Simscape library is used. Model illustration and its main parameter setting are showed in Figure 30.

This model uses mainly parameters that are provided by public data such as rated power (2.5MVA), electrical frequency (f), primary/secondary voltage (V_LV, V_HV). These parameters are hence used in the model. Moreover, winding resistance from both primary and secondary sides are needed. The later represent transformer's losses, essentially during loaded operation, i.e. when transformer is in closed circuit. These parameters are important for transformer's efficiency and related voltage losses modelling. As no manufacture data is provided for these parameters, primary winding resistance and secondary winding resistance are fixed at 0.01 p.u. These values, although not precis, fit to CEI EN 50464-1 standard on transformers with voltage ranged up to 24kV [18].

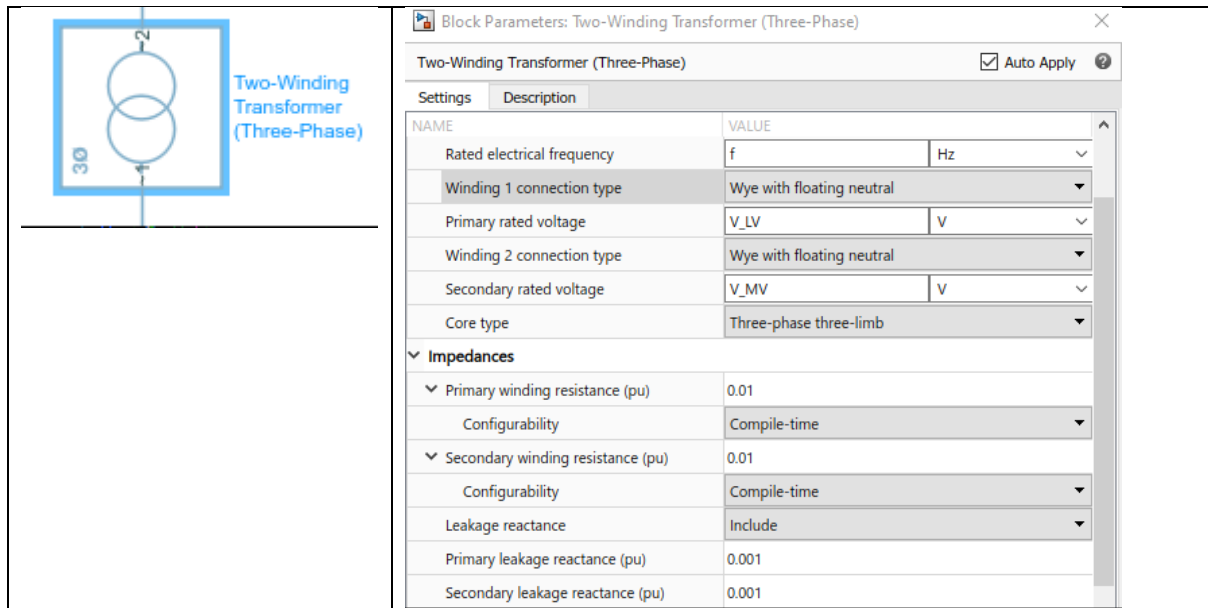


Figure 30 Transformer model and parameters.

5.2.2.5 Loads

Two groups of loads are represented in the model: the port's building consumption and future electrical vehicle charging load. Each of them is an aggregation of smaller loads, which are not modelled in detail. For both models, dynamic balanced load model is used. This model's parameter setting is quite simple, with the following elements:

- Time series data for active power (P input) and reactive power (Q input)
- Minimum supply voltage and minimum active power. These values can be considered as model's boundary, from which load's consumption active and reactive power are equal to those specified by the time series P and Q inputs. If the load's voltage and power are lower than these limits, this model behaviour changes to a constant impedance load. Model parameter illustration is presented in Figure 31.

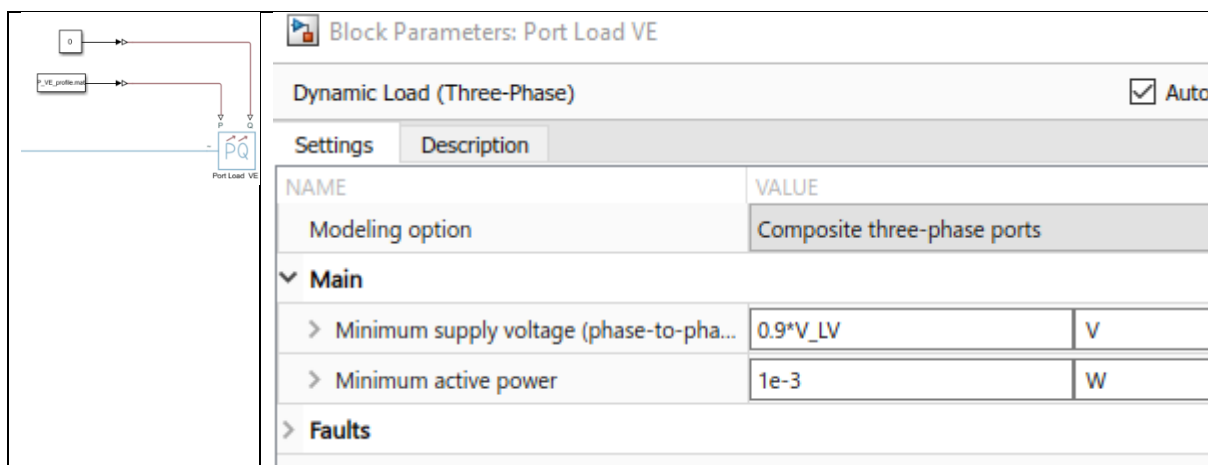


Figure 31 Dynamic load model.

5.2.2.6 Parameter table

In Table 9, all parameter used for grid model are listed. For simulation purposes, the values to the line resistance and reactance were changed by arbitrary values.

Table 9 Grid parameters.

Grid Parameters	Value and Unit
Nominal frequency, f	50 Hz
Medium voltage phase to phase, V_{MV}	20000 V
Low voltage phase to phase, V_{LV}	400 V
Line resistance (420m line)	0.0865 Ohm
Line reactance (420m line)	$1,3020 \times 10^{-4}$ Henry
Line resistance (590m line)	0.1215 Ohm
Line reactance (590m line)	$1,8290 \times 10^{-4}$ Henry
Transformer nominal power, P_{Transf}	2.5e6 VA
Building load active power, $P_{LoadPort}$	2e4 W
Building load reactive power, $Q_{LoadPort}$	0 VAR
Time and active power vector of EV charging load, T_{VE}, P_{VE}	Depending on EV charge profile, s,W
PV installed power, P_{PV_Peak}	1.7e6 W
Time and active power vector of PV production, T_{PV}, P_{PV}	Depending on PV production profile, W

5.2.2.7 Grid model inputs and outputs

The main responsibility in the grid model is to provide the available power for charging. This will be influenced by the inputs provided in the form of the extra PV power available, the grid

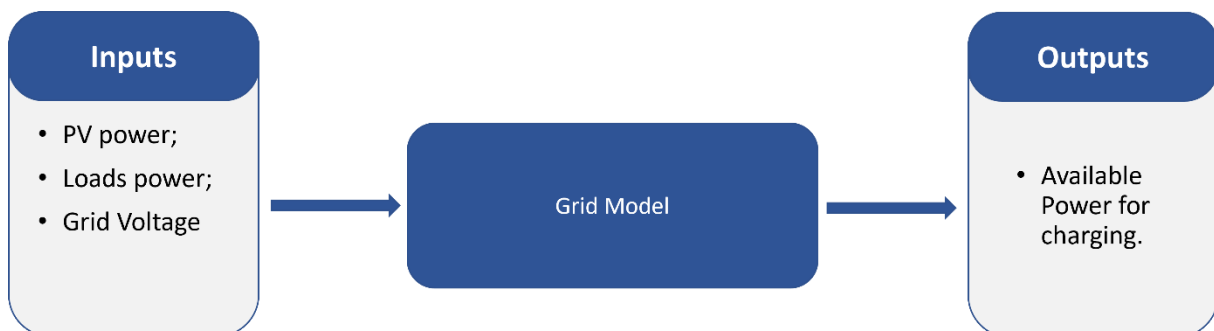


Figure 32 Grid model inputs and outputs.

voltage and the current loads in the port. All combined will give an overall availability of power to the charger to operate.

6. DIGITAL TWIN AND USE CASES EXAMPLE

The end result is a model representative of three components working together, which can be seen in Figure 33 Simulink model of the digital twin of the whole system. The generalized thermal port for the convection is shared with the battery and the charger model, while electric connectivity is established between all three models. The charging profile will represent the input of the EMS when it is developed and will manipulate the 3 represented inputs, charging the battery accordingly. In this case, for model testing, user defined charging profiles were provided. All the general parameters of the battery for the simulation are presented in Table 10 Battery parameters used in the use cases.

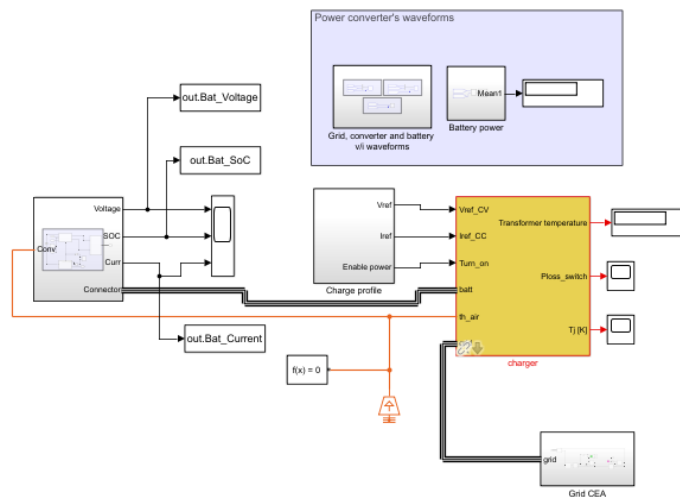


Figure 33 Simulink model of the digital twin of the whole system.

To further expose the DT operation, charging test runs were done. These naturally consider values that do not fully represent the final system and are subject to change. Two case scenarios are presented: charge after a full turnaround and after 1.5 turnarounds. As explained in D1.4, the worst-case scenario would need 2.1 MW worth of output power from the charger to fully charge the battery in 30 minutes. Even in the worst-case scenario, the evaluation done lead to believe that given the max C-Rate in the worst-case scenario to be just shy of 1.5C, so for the current moment CC-CV charging profile will be used. Current, voltage and SoC will be presented for both cases.

Table 10 Battery parameters used in the use cases.

Battery parameters	Value
SoC	50%/25%

Battery Capacity	1545 Ah
Charge Load Profile	[1500-800] A / [2100-500] A

Two random current profiles were used for demonstration purposes. For the best-case scenario was the vessel is charged in every mooring event, it is clear that it is not necessary to exceed 1C rate. There is a lot of margins to establish some more conservative charging rates to further enhance battery life. In the second case a full charge was not attained with the used current profile. There is clear room for adaptation and change in search of the optimal charging strategy, including the effects of aging, which will be achieved later into the project. But this provides a baseline for future work.

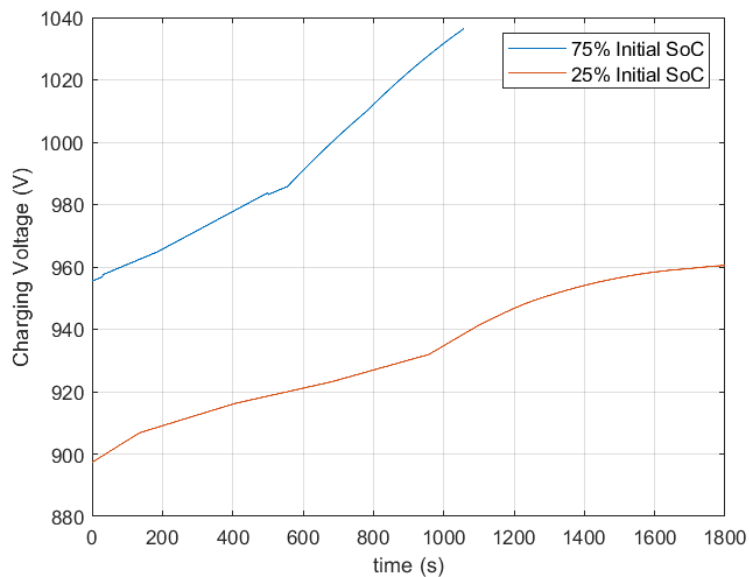


Figure 34 Voltage behaviour for the two use cases.

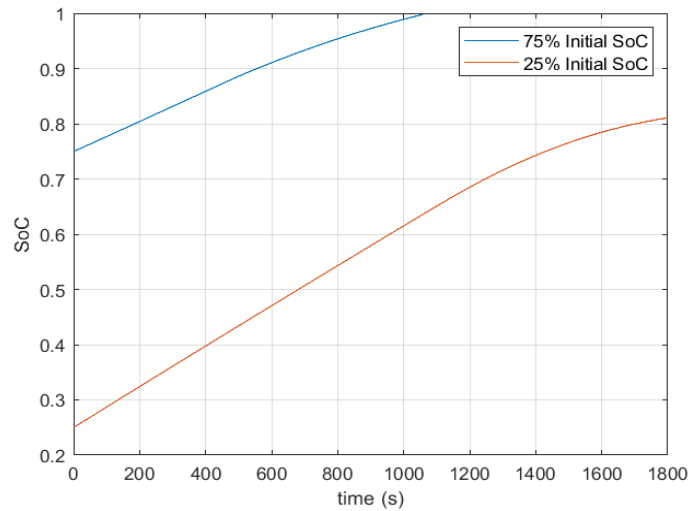


Figure 35 SoC evolution for the two use cases.

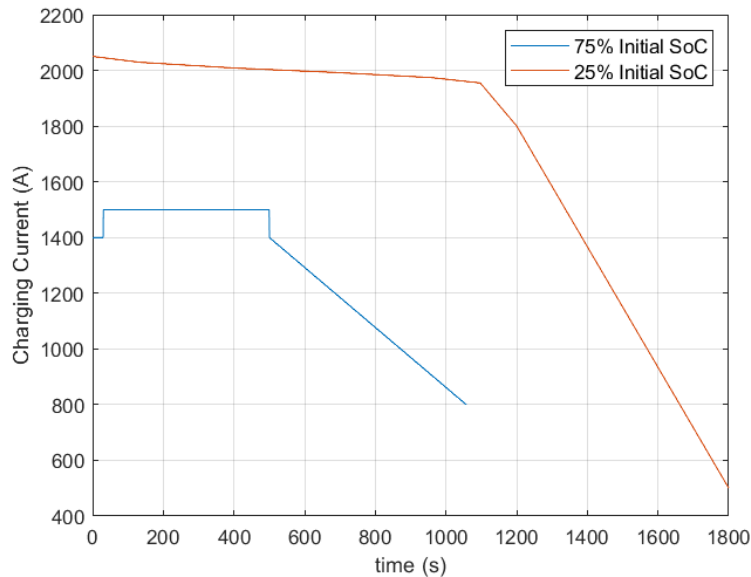


Figure 36 Charging current profile used in the two use cases.

7. CONCLUSIONS

In this work the first iteration of the DT of the charging system is presented. This is represented by the offshore and on shore models, with the offshore being represented by the battery system of the vessel and the on shore the combination of the AC/DC converter, transformer and grid models. Each with its own degree of complexity, the combination results in an algorithm capable of simulating a charging event, independent of the scenario. Given that this

will be a slave to the EMS algorithm, its main function was accessed and demonstrated to work in the intended manner. A more thorough use case approach will be done further down in the projects time, with the full EMS application and control of the charging algorithm with respects to the battery and charger boundary conditions and the macro restrictions financially and logistically wise.

With the whole system implemented in a cloud platform, the DT will allow the charger operators to fully maximize the potential of the physical system by testing multiple scenarios and conditions, allowing to maximize battery life and minimize operation costs.

8. REFERENCES

- [1] J. B. H. X. L. X. W. X. P. M. Dai H, "Advanced battery management strategies for a sustainable energy future: Multilayer design concepts and research trends.," *Renewable and Sustainable Energy Reviews*, 2021.
- [2] T. J. S. Z. W. L. X. R. L. M. C. Z. Wang Y, "A comprehensive review of battery modeling and state estimation approaches for advanced battery management systems.," *Renewable and Sustainable Energy Reviews*, 2020.
- [3] W. J. T. J. L. J. X. R. Wang W, "Application of digital twin in smart battery management systems.," *Chinese Journal of Mechanical Engineering.*, pp. 1-9, 2020.
- [4] "Heat-generation rate and general energy balance for insertion battery systems.," *Journal of the Electrochemical Society*, 1997.
- [5] J. d. H. M. B. A. V. a. S. V. Muenzel, "A Multi-Factor Battery Cycle Life Prediction Methodology for Optimal Battery Management," in *ACM Sixth International Conference on Future Energy Systems*, Bangalore, India, 2015.
- [6] N. N. S. K. J. S. H. B. A. W. a. D. U. S. M. Ecker, "Calendar and cycle life study of Li(NiMnCo)O₂-based 18650 lithiumion batteries.," *Journal of Power Sources*, vol. 248, pp. 839-851, 2014.
- [7] "INVADE, H2020 project, D6.4 Advanced state of health diagnostics tool."
- [8] R. P. ., L. K. A. T. Damian Burzyński, "Analysis and Modeling of the Wear-Out Process of a Lithium-Nickel-Manganese-Cobalt Cell during Cycling Operation under Constant Load Conditions," *Energies*, vol. 12, p. 3899, 2019.
- [9] J. A. Martinez-Velasco, *Power System Transients Parameter Determination*, 2009.
- [10] *IEEE Standard Test Code for Liquid-Immersed Distribution, Power, and Regulating Transformers*, in *IEEE Std C57.12.90-2015 (Revision of IEEE Std C57.12.90-2010)* , vol., no., pp.1-120, 11 March 2016, doi: 10.1109/IEEESTD.2016.7428800..
- [11] S. a. C. H. Churchill, ""Correlating Equations for Laminar and Turbulent Free Convection from a Horizontal Circular Cylinder," *International Journal of Heat and Mass Transfer*, vol. 17, pp. 1323-1329, 1974".
- [12] H. K. N. Asadi, ""Modeling, analysis, and detection of internal winding faults in power transformers", *IEEE Trans. Power Delivery* 30 (6) (2015) 2419–2426."

-
- [13] K. H. H. H. J. Z. H. Zhou, ""Transformer winding fault detection by vibration analysis methods", *Applied Acoustics* 114 (2016) 136–146."
- [14] Mathworks, "Cauer Thermal Model," [Online]. Available: <https://es.mathworks.com/help/sps/ref/cauerthermalmodel.html>. [Accessed 2023/01/30].
- [15] Nexans, "Nexans cable datasheet," [Online]. Available: <https://www.nexans.fr/.rest/catalog/v1/product/pdf/10265221>. [Accessed 2022].
- [16] SMA, "SMA PV Inverter datasheet," [Online].
- [17] M. Z. S. F. B. Y. Y. A. Q. Al-Shetwi, "Fault ride-through control of grid-connected photovoltaic power plants: A review," *Solar Energy*, vol. 180, p. 340350, 2019.
- [18] ABB, "Technical guide The MV/LV transformer substations (passive users)," [Online]. Available: https://new.abb.com/docs/librariesprovider27/default-document-library/abb-transformerstations_ebook.pdf?sfvrsn=2.
- [19] J. S. J. S. K. J. C. C. H. K. a. N. H. C. Song, ""Determination method for zero-sequence impedance of 3-limb core transformer."," 2019.
- [20] S. Rivera, R. Fuentes, S. Kouro, T. Dragicevic and B. Wu, "Bipolar DC Power Conversion: State-of-the-Art and Emerging Technologies," *EEE Journal of Emerging and Selected Topics in Power Electronics*, pp. 1-1, 2020.
- [21] Mathworks, "Loss Calculation in a Three-Phase 3-Level Inverter," 2022. [Online]. Available: <https://es.mathworks.com/help/sps/ug/loss-calculation-in-a-three-phase-3-level-inverter.html>.
- [22] Mathworks, "Converter (Three-Phase)," 2022. [Online]. Available: https://es.mathworks.com/help/sps/ref/converterthreephase.html?searchHighlight=Converter%20%28Three-Phase%29&s_tid=srchtitle_Converter%20%2528Three-Phase%2529_1.
- [23] R. X. a. J. F. H. He, "Evaluation of Lithium-Ion Battery Equivalent Circuit Models for State of Charge Estimation by an Experimental Approach," *Energies*, vol. 4, no. 4, p. 582–598, Mar. 2011.
- [24] A. L. A. C. A. A. S. a. P. V. R. Abdelhedi, "Reinforcement learning for the control of battery electrothermal behaviours in electric vehicles," *Turkish Journal of Electrical Engineering and Computer Sciences*, Oct. 2018.